

CHROMATIN ORGANIZATION IN THE SMALLEST  
FREE-LIVING EUKARYOTE *OSTREOCOCCUS TAURI*

SONG YAJIAO

*(BSc., Life Sciences)*

*A THESIS SUBMITTED*

*FOR THE DEGREE OF MASTER OF SCIENCE*

*DEPARTMENT OF BIOLOGICAL SCIENCES*


*NATIONAL UNIVERSITY OF SINGAPORE*

2014

# Declaration

I hereby declare that the thesis is my original work and it has been written by me in its entirety. I have duly acknowledged all the sources of information, which have been used in the thesis.

This thesis has also not been submitted for any degree in any university previously.



---

SONG YAJIAO

16 December 2014

## **Acknowledgements**

I would like to thank my supervisor Dr. Lu Gan for his patient mentoring and for his helping in designing this project. Without his support and guidance, I would never have carried on to finish this thesis. His encouragement has always been my motivation to come over the difficulties and challenges. Being in his lab is one of the best experiences in my life.

I would also like to thank my labmate and best friend Chen Chen for his support and instructions. Without him, the way to study cryo-EM would have been much harder and painful. I'd also like to thank my labmates Ng Cai Tong, Tay Bee Ling and Yeat Qi Zhen for their kind support.

I would also like to thank Jian Shi, Tran Bich Ngoc and other staffs from Cryo-EM facility for their technical support. The training and guidance from Jian and Ann made this project possible. They were always kind to help when problems came up.

## Table of Contents

Acknowledgements .....	i
Table of Contents .....	ii
Summary .....	iv
List of Tables .....	v
List of Figures .....	vi
List of Abbreviations .....	viii
Chapter 1. Introduction .....	1
1.1 The hierarchy of chromatin organization.....	1
1.2 The 30 nm fiber structure---evidence revisited .....	3
1.2.1 <i>in vitro</i> experiments using extracted chromatin .....	4
1.2.2 <i>in situ</i> experiments using sections from cells .....	9
1.2.3 <i>in vitro</i> experiments using reconstituted oligonucleosomes	10
1.3 The debate about 30 nm chromatin fiber---evidence reexamination .....	17
1.3.1 Evidence from extracted chromatin fiber .....	17
1.3.2 Evidence from <i>in situ</i> experiments .....	22
1.3.3 Evidence from reconstituted oligonucleosomes .....	24
1.3.4 Problems with conventional TEM methods .....	25
1.4 Cryo-EM in chromatin structural studies .....	30
1.4.1 Cryo-EM technique.....	30



1.4.2 Cryo-EM in chromatin structure study .....	33
1.5 Chromatin study in <i>Ostreococcus tauri</i> .....	38
Chapter 2. Materials & Methods .....	44
2.1 Cell growth and preparation for plunge-freezing .....	44
2.2 Plunge-freezing .....	46
2.3 Cryo-ET and image processing .....	47
Chapter 3. Results and discussion .....	49
3.1 Induced 30 nm chromatin fiber .....	49
3.2 Identification of <i>O. tauri</i> nucleus.....	52
3.3 Formation of the 30 nm chromatin fiber with 1mM Mg <sup>2+</sup> .....	55
3.4 30 nm chromatin fiber could be maintained without external Mg <sup>2+</sup> .....	58
3.5 Decondensation of chromatin in 5mM EDTA.....	60
3.6 Polymer melt model of <i>O. tauri</i> chromatin.....	65
Chapter 4. Future Work .....	69
References .....	71

## Summary

Despite the central role of chromatin in many important cellular activities like transcription and DNA replication, how chromatin is organized inside the nucleus *in vivo* remains a topic under hot debate. The 30 nm fiber structure of chromatin has long been considered as one important level of chromatin condensation in heterochromatin and mitotic chromosomes. However, recent cryo-EM studies suggested that the 30 nm fiber structure is absent from both interphase and mitotic cells. Based on these cryo-EM studies, the “polymer melt” model was brought up. We have tested the polymer melt model in the smallest known, free-living eukaryote, *Ostreococcus tauri*, using cryo-electron tomography. Our results confirmed the prediction by the polymer melt model that the disordered nucleosomes *in vivo* could be induced into 30 nm fibers if the chromatin was diluted in a low-salt buffer. This conclusion, which helps us better understand the interactions between nucleosomes, also provides an explanation for the reason that 30 nm chromatin fiber was observed in previous studies. The highly flexible nature of nucleosome organization revealed by our experiments has important implications for uniting the structural basis of chromatin with the regulation mechanisms behind complex genome functions.

## List of Tables

<b>Table 1.</b> $\text{Ca}^{2+}$ and $\text{Mg}^{2+}$ concentrations in interphase and mitotic cells	22
<b>Table 2.</b> ASW composition.....	45
<b>Table 3.</b> Sea salt composition.....	46
<b>Table 4.</b> Electron Tomography Parameters for <i>O.tauri</i> cells treated with 1 mM $\text{Mg}^{2+}$ , 0 mM $\text{Mg}^{2+}$ and 5 mM EDTA. ....	48

## List of Figures

<b>Figure 1.</b> The hierarchy of chromatin organization. ....	2
<b>Figure 2.</b> Finch and Klug’s solenoid model.....	5
<b>Figure 3.</b> Zigzag conformation of extracted chromatin .....	8
<b>Figure 4.</b> Cryo-EM images of Vps4p before (A) and after (B) fixation .	12
<b>Figure 5.</b> Models of the 30 nm chromatin fiber .....	16
<b>Figure 6.</b> 30 nm chromatin fiber were formed in low-salt conditions. ...	22
<b>Figure 7.</b> Obscuration of fine structures by negative staining.....	28
<b>Figure 8.</b> Comparison of conventional TEM and cryo-EM methods ....	29
<b>Figure 9.</b> Summary of cryo-ET.....	33
<b>Figure 10.</b> Cryosection of a HeLa cell.....	35
<b>Figure 11.</b> Polymer melt model.....	37
<b>Figure 12.</b> 3D ultrastructure of <i>O. tauri</i> .....	39
<b>Figure 13.</b> <i>O. tauri</i> chromatin is not organized as 30 nm fibers.....	41
<b>Figure 14.</b> Steps to induce 30 nm chromatin fiber in <i>O. tauri</i> .....	50
<b>Figure 15.</b> Low-magnification cryo-EM image of lysed, frozen-hydrated <i>O. tauri</i> cells. ....	52
<b>Figure 16.</b> Identification of <i>O. tauri</i> nucleus .....	53
<b>Figure 17.</b> 28 nm tomographic slices of partially lysed <i>O. tauri</i> cells treated with 1 mM Mg <sup>2+</sup> .....	54
<b>Figure 18.</b> Polymer melt state of nucleosomes in lysed <i>O. tauri</i> cells treated with 1 mM Mg <sup>2+</sup> . ....	56
<b>Figure 19.</b> Formation of 30 nm chromatin fiber in lysed <i>O. tauri</i> cells treated with 1 mM Mg <sup>2+</sup> . ....	57

<b>Figure 20.</b> 30 nm chromatin fibers were maintained in lysed <i>O. tauri</i> cells without external Mg <sup>2+</sup> .....	59
<b>Figure 21.</b> Decondensed chromatin of lysed <i>O. tauri</i> cells treated with 5 mM EDTA.....	61
<b>Figure 22.</b> Nucleosome densities from decondensed chromatin.....	62
<b>Figure 23.</b> 10 nm nucleosomal fibers in lysed <i>O. tauri</i> cells treated with 5 mM EDTA.....	63
<b>Figure 24.</b> Partially decondensed 30 nm chromatin fiber in 5 mM EDTA .....	64
<b>Figure 25.</b> Chromatin conformation at different conditions. ....	67

## List of Abbreviations

### Chemicals and Reagents

ASW	artificial sea water
EDTA	ethylenediaminetetraacetic acid
HEPES	4-(2-Hydroxyethyl) piperazine-1-ethanesulfonic acid
MgCl <sub>2</sub>	magnesium chloride
NaCl	sodium chloride

### Units and Measurements

bp	base pairs
g	gram
K	Kelvin
kV	kilovolt
L	liter
Mb	million base pairs
mg	milligram
ml	milliliter
mM	millimolar
nm	nanometer
nM	nanomolar
s	second
v/v	volume per volume
Å	angstrom
°	angular degree
°C	degree Celsius
e <sup>-</sup> /Å <sup>2</sup>	electron per square angstrom

$\mu\text{m}$	micrometer
$\mu\text{g/ml}$	microgram per milliliter

### **Others**

CTF	contrast transfer function
cryo-EM	cryo-electron microscopy
cryo-ET	cryo-electron tomography
DNA	deoxyribonucleic acid
EM	electron microscopy
ET	electron tomography
OD	optical density
TEM	transmission electron microscopy
RNA	ribonucleic acid

## Chapter 1. Introduction

### 1.1 The hierarchy of chromatin organization

W. Flemming first described chromatin around 1882 [1]. However, 130 years have passed and the structural organization of chromatin *in vivo* still remains an active area of research. The basic repeating unit of chromatin is the nucleosome core particle, in which 146 bp of DNA wraps around a histone octamer [2]. The octamer is composed of the 4 different core histones, H2A, H2B, H3 and H4, each in two copies [3]. Nucleosome core particles are connected by linker DNA associated sometimes with the linker histone called H1[4, 5]. Nucleosomes, together with the linker DNA, form a 10nm-thick structure, which is called the “beads-on-a-string” structure (Figure 1) [3, 6].

The 10 nm “beads-on-a-string” was first reported to form a higher order structure, which was also a fiber-like structure of 30 nm in diameter, in purified chromatin[7]. Since then, other research groups had observed the 30 nm chromatin fiber in various systems[8-17], resulting in the 30 nm fiber structure becoming a textbook model as a secondary chromatin structure. Until now, many research groups used this 30 nm fiber model to help design experiments and to interpret data [18-20]. Although the structural details of the 30 nm chromatin fiber



have been under debate since it was discovered, the idea that the 10 nm chromatin fibers first organize into 30 nm fiber and then this 30 nm fiber can further pack into higher order, condensed structures in mitotic chromosomes or in heterochromatin, is widely accepted (Figure 1).

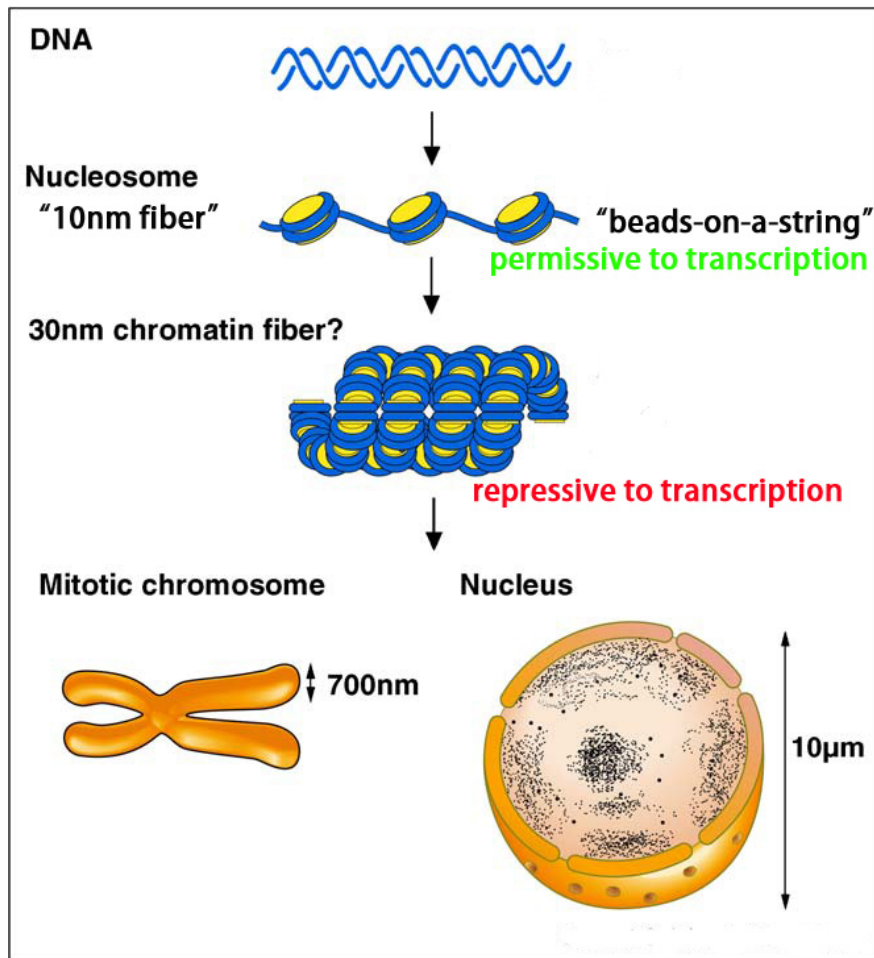


**Figure 1.** The hierarchy of chromatin organization (adapted from **Maeshima *et al.*, 2010**) [21]. DNA wraps around the histone octamers, forming the 10 nm fiber. The 10 nm fiber has long been assumed to first fold into the 30 nm chromatin fiber and then the 30 nm fiber further folds into higher order structures of mitotic chromosomes or interphase heterochromatin.

To explain chromatin organization above the 30 nm chromatin fiber level, many models have been put forward, for example, the “hierarchical helical folding” model [22] or the “radial loop” model[23-25]. In the “hierarchical helical folding” model, 30 nm chromatin fibers first coil into a super-solenoid fiber and this super-solenoid fiber then forms the highly condensed mitotic chromosomes. In the “radial loop model”, the 30 nm fibers fold into radially oriented loops to form mitotic chromosomes. Although these models differ from each other in the organization form of higher (above the 30 nm fiber level) order chromatin structure, they share the assumption that the 30 nm fiber structure exists in mitotic cells and that the 30 nm fiber is the basic organization form of chromatin higher order structures.

Since the first description of the 30 nm fiber came up, this structure was also suggested to play a regulatory role in gene transcription. It was proposed that the 30 nm fiber was the organizing form of transcriptionally silent genes [7, 26, 27]. Because of its important role in the proposed hierarchy of chromatin organization and its potentially regulatory role in gene transcription, the structure of the 30 nm chromatin fiber was extensively studied over the past three decades.

## **1.2 The 30 nm fiber structure---evidence revisited**

Considering the dimensions and the complexity associated with chromatin organization, transmission electron microscopy (TEM) has been the best approach to study 30 nm chromatin fibers. Conventional TEM, in which the samples are preserved at room temperature by chemical treatments, contributed a lot to the establishment of the 30 nm fiber model. Other studies also detected the 30 nm fiber using methods like cryo-electron microscopy (cryo-EM) and electric dichroism[16, 17][10, 16]. All the experiments that supported the existence of the 30 nm chromatin fiber can be divided into 3 categories based on the materials used in the experiments:

### **1.2.1 *in vitro* experiments using extracted chromatin**

The first description of the 30 nm fiber model was based on Finch and Klug's observation of extracted chromatin[7]. Since then, the *in vitro* system using extracted chromatin has become a popular method to study chromatin organization.

In Finch and Klug's experiment, chromatin was extracted from rat liver nuclei[7]. The cells were lysed in hypotonic buffer, and then the nuclei were isolated and treated with nuclease to cut the chromatin into fragments. After the nuclease treatment, the nuclei were resuspended in a low-salt buffer and the chromatin fragments were then released due to the hypotonic shock [28]. The extracted chromatin fragments

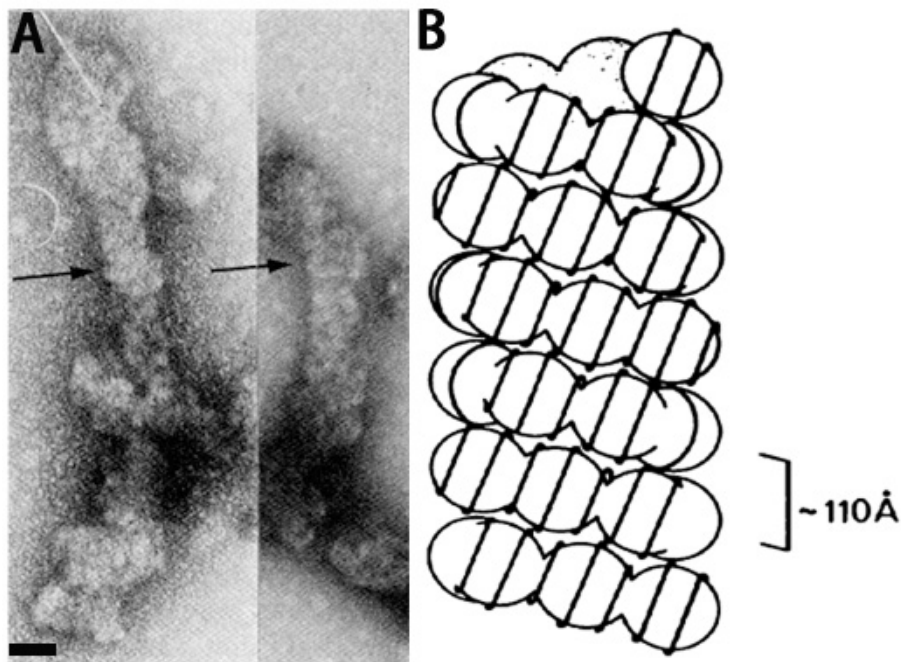


**Figure 2. Finch and Klug's solenoid model (adapted from Finch and Klug, 1976)[7].** (A) TEM images of negatively stained chromatin extracted from rat liver nuclei, with the presence of 0.5 mM  $Mg^{2+}$ . Arrows indicate transverse striations across the 30 nm fiber. Scale bar, 30 nm. (B) Solenoid model of 30 nm chromatin fiber. The helix along the nucleosome fiber represents the DNA on the outside of a histone octamer. The model is highly schematic since the DNA path is unknown.

were then negatively stained and imaged in the TEM at room temperature. In the presence of more than 0.2 mM  $Mg^{2+}$ , the dominant form of chromatin structure was found to be a 30 nm fiber structure. Results from this experiment suggested that the 30 nm fiber structure was formed by winding up the 10 nm nucleosome fiber into helices and that the formation of the 30 nm fiber structure was highly dependent on  $Mg^{2+}$  concentration and H1 linker histones. Based on their results, Finch and Klug put forward the first variant of the 30 nm chromatin fiber

-the solenoid model. In their schematic model, consecutive nucleosomes are positioned next to each other in the fiber, folding into a helix (Figure 2).

Other researchers using extracted chromatin basically followed the same extraction procedures, which included cell lysis by hypotonic shock or detergent treatment, nuclease treatment and low-salt treatment to nuclei. Similarly, using chromatin extracted from rat liver cells, Thoma *et al.* further investigated the progressive formation of the 30 nm fiber with increasing ionic strength in a series of artificial buffers [8]. The 30 nm fiber structure could be formed with the presence of 60 mM monovalent salt (or else a low concentration of divalent salt like  $\sim 0.3$  mM  $Mg^{2+}$ ). The helical path of the 30 nm fiber was also resolvable in their TEM images. Negative stained chromatin from metaphase mouse L929 cells also tended to form the 30 nm fiber structure and the stability of the 30 nm fiber varied according to variations in cell lysis conditions. The 30nm fiber structure derived from detergent-lysed cells appeared to be less stable than chromatin fibers obtained by mechanically lysed cells [9]. McGhee *et al.* used electric dichroism to study chromatin extracted from chicken erythrocytes. The nucleosomes in the chromatin fragments were oriented by a strong electric field. By applying polarized light parallel to the direction of the electric field and polarized light perpendicular to the direction of the electric field, they could compare the difference in the absorbance of

the two polarizations of light by the DNA in the nucleosomes and then calculate the possible orientation of both the linker DNA and the DNA wrapped around the histone core. The relaxation time of the dichroism signal from the  $Mg^{2+}$ -condensed chromatin matched the expected time from a 30 nm solenoid [10]. The solenoid model has been greatly developed by these studies since it was first brought up in 1976 and has become the major model describing the conformation of the 30 nm chromatin fiber.

The zigzag model is another variant of the 30 nm fiber models. Worcel *et al.* extracted chromatin fragments from embryonic chicken erythrocytes. They used formaldehyde and uranyl acetate to fix the extracted chromatin and then shadowed the chromatin with platinum-carbon. The partially unraveled chromatin appeared to be “two-stack” arrays in which the linker DNA went back and forth in a zigzag manner. Based on the observation, they put forward the zigzag ribbon model. Also using conventional EM method, Woodcock *et al.* observed chromatin extracted from mouse fibroblast cells and chicken lymphoblastoid cells prepared using different techniques including negative staining and platinum-carbon shadowing [29]. With the presence of 10 mM NaCl or 0.01 mM  $MgCl_2$ , both the full-length chromatin and the chromatin fragments showed a compact fiber structure formed by zigzag folding of nucleosomes. The width, pitch angle and the gyre spacing of the compact fiber were measured.

Based on these measurements, a model describing the structural details of the 30 nm chromatin fiber was also proposed. Bednar *et al.* extracted chromatin from chicken erythrocyte cells and COS-7 cells and studied the chromatin structure by cryo-EM [11, 17]. They also observed the 30 nm fiber structure existing in a zigzag conformation. In their zigzag model (Figure 3), alternate nucleosomes are interacting partners rather than consecutive nucleosomes in the solenoid model. The zigzag model and the solenoid model have now become two major models that explain the conformation of the 30 nm chromatin fiber.

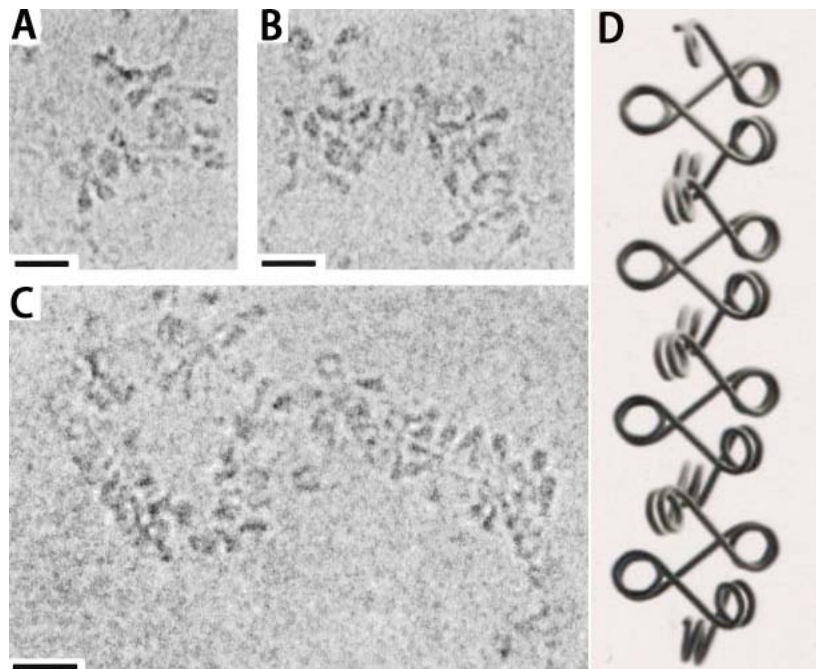


**Figure 3. Zigzag conformation of extracted chromatin (adapted from Bednar *et al.*, 1998)[17].** (A-B) Cryo-EM images of chromatin extracted from COS-7 cells vitrified in 40 mM Na<sup>+</sup> (C) Extracted chromatin of chicken erythrocytes imaged in 15 mM Na<sup>+</sup>. The zigzag conformation could be recognized of chromatin from both types of cells. (D) Schematic zigzag model of 30 nm chromatin fiber. Scale bar, 30 nm.

### 1.2.2 *in situ* experiments using sections from cells

With the development of TEM sample preparation methods, especially the low temperature methods, scientists were able to study chromatin structure *in situ* inside the nuclei. These *in situ* studies of chromatin structure were considered to better represent chromatin structure *in vivo*.

Woodcock first observed the 30 nm fiber structure in frozen-hydrated sections of three types of cell nuclei, chicken erythrocytes, sperm of *Patiria miniata* (starfish) and *Thyone briareus* (sea cucumber) [14]. Nuclei from all three types of cells were filled with well-resolved chromatin fibers of a diameter around 30 nm. Combining low temperature embedding and electron tomography (ET), Horowitz *et al.* also studied the 3D structure of chromatin fibers in sections of chicken erythrocyte nuclei and sperm from *Patiria miniata* [15]. They were able to determine the 3D trajectories of a number of clearly defined 30 nm fibers. They found that a common structural motif of the 30 nm chromatin fiber was a twisted ribbon-like array of nucleosomes. The zigzag path of consecutive nucleosomes was twisted due to variations of linker DNA length and the entry-exit angle of the linker DNA. In a more recent study, using cryo-electron tomography (cryo-ET) Scheffer *et al.* also showed that the most predominant form of chromatin in



chicken erythrocyte nuclei was the 30 nm fiber structure, which was a two-start helix [16]. Results from these *in situ* experiments provided additional support for the existence of the 30 nm chromatin fiber *in vivo*.

### **1.2.3 *in vitro* experiments using reconstituted oligonucleosomes**

While studies based on chromatin from cells, either extracted or *in situ*, have made great progress, there are still some problems that prevent these studies from achieving a high-resolution structure of the chromatin conformation. Most of the previous studies showed that the length of the linker DNA between nucleosomes had an important influence on the formation of the 30 nm fiber structure [12, 13]. But *in vivo*, the length of the linker DNA varies in a large range thus the 30 nm chromatin fiber formed either *in situ* or using extracted chromatin was highly variable. Other factors like DNA sequences and different histone modifications may also contribute to structural heterogeneity of the 30 nm chromatin fiber.

The heterogeneity of sample is usually the main obstacle to achieving a structure of high resolution. Yu *et al.* used cryo-EM single particle analysis to study the structure of yeast Vps4p complex, which is a type I AAA (ATPase associated with a variety of cellular activities) ATPase [30]. Only after the purified Vps4p complexes were fixed with 0.02% glutaraldehyde for 20 minutes and repurified afterwards by size-

exclusion chromatography, could they obtain cryo-EM images with protein complexes uniformly distributed in the field of view (Figure 4B). Otherwise most regions of the grids showed either clear ice without the complexes or protein aggregates (Figure 4A). Elution profile of the size-exclusion chromatography and SDS-PAGE analysis showed an obvious decrease in heterogeneity of the sample after glutaraldehyde fixation compared with unfixed sample. One possible explanation for the differences was that the flexible domains in the complex that have caused the aggregation have been immobilized by the fixation, meanwhile native conformational heterogeneities due to these flexible domains were also diminished. Thus, the conformations that were observed after the fixation could not faithfully reflect all the native conformations of the complexes. The fixation might transform many different conformations into only a small subset of conformations, which we call “fixation-biased” conformations and they were still a subset of native conformations or in a worse case, the fixation might change the native structures, resulting in what we call “fixation-modified” conformations, which were artifactual. Aldehyde fixation (0.2% glutaraldehyde treatment for 30 minutes) was also applied to reconstituted nucleosome arrays in a recent study by Song *et al.* that reported an 11Å-resolution cryo-EM structure of the 30 nm chromatin fiber [31]. Unfortunately, the authors did not show any data of how heterogeneous the nucleosome arrays were before fixation. Therefore, from the different behaviors of unfixed and fixed samples in the study

of yeast Vps4p complex, it should be noticed that great caution must be taken when interpreting structures from fixed samples that are intrinsically heterogeneous.

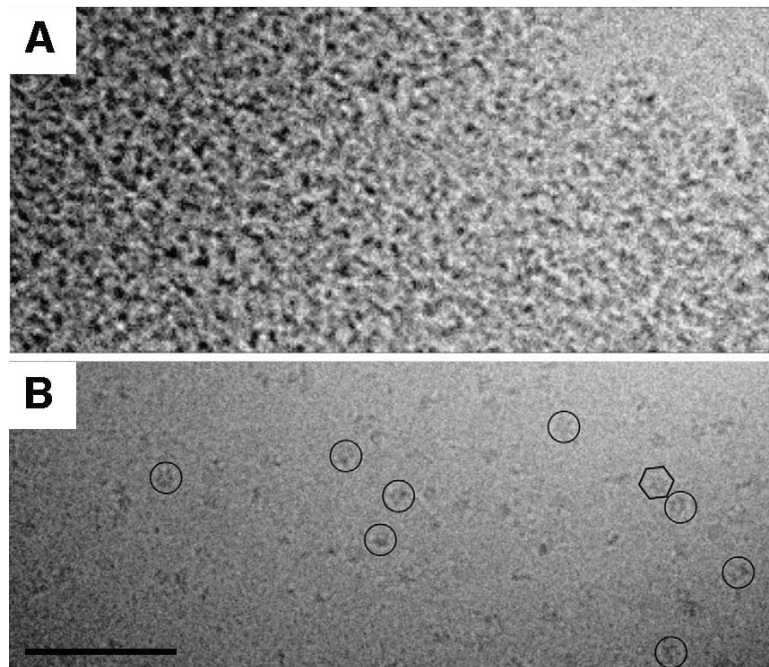


**Figure 4. Cryo-EM images of Vps4p before (A) and after (B) fixation (adapted from Yu *et al.*, 2008) [30].** The circles indicate individual Vps4p particles and the hexagon indicates one Vps4p complex with visible hexagonal symmetry. Scale bar, 100 nm.

To overcome the problem caused by sample heterogeneity, some researchers tried to use biochemically well defined, reconstituted nucleosome arrays to study the internal organization of the 30 nm chromatin fiber structure. These reconstituted nucleosome arrays were based on 5S ribosomal DNA repeats [32] or clone 601 “Widom” DNA selected from random synthetic DNA sequences[33]. The DNA sequences of the reconstituted nucleosomes and the linker DNA were

known and had the characteristic of precise positioning of histone octamers. Indeed, results from structural studies using reconstituted nucleosome arrays had improved precision compared with those *in situ* studies or studies using extracted chromatin.

Huynh *et al.* reported an *in vitro* chromatin reconstitution system, which used 12 and 19 copies of the 601 DNA sequence [34]. They added a competitor DNA in the reconstitution to control the stoichiometry of the linker histones and the nucleosomes. By screening a number of buffer conditions, they established an optimized condition for the reconstituted nucleosome arrays to form a compact fiber structure. Both negative staining and cryo-EM of the folded arrays showed a homogeneous population of a fiber structure, with a uniform diameter of 34 nm. Using nucleosome 12-mer arrays of the 601 sequence, Grigoryev *et al.* examined the influence of linker histones and  $Mg^{2+}$  ions on the formation of the compact 30 nm chromatin fiber [35]. To better understand the dynamics of chromatin structural change, they established a method called EM-assisted nucleosome interaction capture (EMANIC), in which they used formaldehyde cross-linking to fix the contacts between nucleosomes in the 30 nm fiber structure. Their results showed that the linker histones promote the formation of a two-start zigzag fiber dominated by interactions between alternate nucleosomes while the divalent ions further compact the fiber by promoting bending in the linker DNA. From a dynamic perspective,

they concluded that the two-start zigzag conformation and the type of linker DNA bending that marked the solenoid model might be simultaneously present in the same 30 nm chromatin fiber. Robinson *et al.* produced a series of nucleosome arrays with up to 72 nucleosomes to define the dimensions of the 30 nm chromatin fiber accurately [36] (Figure 5). The arrays were all based on the 601 sequence and the length of the linker DNA in each array was different from each other. The long nucleosome arrays could fold into 30 nm fibers after dialysis into buffers containing 1.0 to 1.6 mM MgCl<sub>2</sub>. Their EM measurements showed that there were two distinct classes of fiber structure, both with high nucleosome density. The reconstituted chromatin fibers were almost twice (about 10-18 nucleosomes per 11 nm) as compacted as generally assumed (about 6 nucleosomes per 11 nm), if the chromatin were in its fully compact state. Because the length of linker DNA and the ratio of linker histone to nucleosomes could be under control in reconstituted nucleosome arrays, the *in vitro* reconstitution system is an important way to study the influence of linker DNA and linker histone on nucleosome compaction.

Another advantage of the reconstitution system is that it could achieve structures of relatively high resolution. Schalch *et al.* solved the X-ray crystal structure of a reconstituted tetranucleosome at 9 Å resolution, based on molecular replacement using the nucleosome core particle (Figure 5). They adjusted the crystallization conditions to

provide the maximum 30 nm fiber compaction. The tetranucleosome used in their experiments was synthesized from four tandem 147 bp copies of the 601 sequence, connected by 20 bp DNA linkers. The histone octamers in the tetranucleosomes were purified from recombinant *Xenopus laevis* histone octamers lacking any post-translational modifications. Their structure showed that the linker DNA formed a zigzag path between 2 nucleosomes and the whole structure was a truncated two-start helix. In the study by Song *et al.*, they reconstituted two kinds of 12-mer nucleosome arrays with different linker DNA length using the 601 DNA sequence and the recombinant *Xenopus laevis* canonical histones without any post-translational modifications [31]. They also incorporated H1 histone in their nucleosome arrays. After several steps of dialysis and prolonged glutaraldehyde fixation, the reconstituted nucleosome arrays were in the form of compact 30 nm fibers. The whole 30 nm fiber had a two-start zigzag conformation and the structural unit of the 30 nm fiber was a tetranucleosome. Within each tetranucleosome, two stacks of two nucleosome cores were connected by straight linker DNA. Studies using reconstituted nucleosome arrays have greatly pushed our understanding of the internal structure of the 30 nm chromatin fiber.

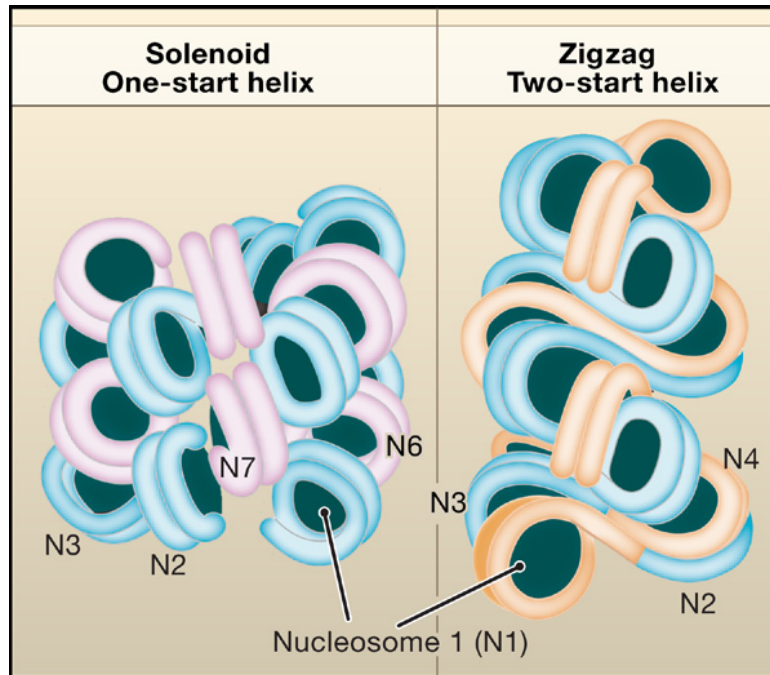


**Figure 5. Models of the 30 nm chromatin fiber (Tremethick, 2007)**

**[37].** (Left) The solenoid model proposed by Robinson and Rhodes. The model is an interdigitated, one-start helix. A nucleosome in the fiber interacts with its fifth and sixth neighbors [36]. Alternative helical gyres are colored blue and magenta. (Right) The zigzag model suggested by Richmond and colleagues. Nucleosomes are arranged into a two-start helix. Alternate nucleosomes form interacting partners [38].

Since Finch and Klug first put forward the 30 nm chromatin fiber as an organization form of chromatin in 1976, many studies have been carried out on the 30 nm fiber model. In most of these studies, the 30 nm chromatin fiber could form and could be detected, supporting the existence of this fiber structure. With such compelling evidence, the 30 nm fiber structure finally became a textbook model to explain how chromatin was compacted inside the small volume of the nucleus [39-41]. The focus of chromatin structure studies has now moved forward to investigate the internal organization of the 30 nm chromatin fiber.

However, as our knowledge in sample preparation and imaging techniques increases, researchers begin to reexamine the results from these earlier studies and debate about the existence of the 30 nm fiber started again.

### **1.3 The debate about 30 nm chromatin fiber---evidence reexamination**

#### **1.3.1 Evidence from extracted chromatin fiber**

When considering results from *in vitro* studies using extracted chromatin, we should pay special attention to several problems: 1) What are the treatments used in the extraction? 2) Will these treatments bring artifacts to the native chromatin structure (“native” here means *in vivo*)? 3) What are the physical factors that have changed, from *in vivo* environment to the relatively simple *in vitro* system?

To extract chromatin from cells, there are usually three basic steps that cannot be avoided. They are: cell lysis, which disrupts the cell membrane and releases the nuclei; chromatin fragmentation, which cuts the chromatin into large fragments to dissolve the viscous mass of chromatin into a homogeneous solution; and nuclei lysis, which



releases the chromatin fragments from the nuclei [7, 8, 15, 28, 29, 42, 43].

For cell lysis, detergent was usually used to disrupt cell membrane. The concentration of the detergent and the lysis time used varied from study to study. It is not clear which lysis design is optimal for retaining native chromatin structure. The influence of detergent on the folding of histone proteins as well as on the interaction between histones and DNA has yet to be investigated. For chromatin fragmentation, micrococcal nuclease was added to the buffer containing the released nuclei; for nuclei lysis, a hypotonic buffer is used to resuspend the nuclei after chromatin fragmentation. The composition of the hypotonic buffer, especially the concentration of monovalent or divalent cations, also varied in different studies.

In a study on the relationship between fragmented chromatin in solution and chromatin in intact nuclei, Giannasca *et al.* found the processes of chromatin fragmentation and nuclei lysis did not simply transfer the native chromatin higher-order structure to the external medium, but induced changes in chromatin organization [44]. In their study, they considered chromatin conformation observed in whole starfish sperm prepared by Tokuyasu method as “native” chromatin conformation. The nuclease fragmentation was examined over a range of ionic strengths and the loss of “native” structure of the chromatin

occurred under all conditions tested. They did not find a condition, which could make the chromatin accessible to the nuclease and at the same time could prevent native chromatin from decondensing and at the same time. They also suggested that even if such a condition could be found, the ionic strengths needed would result in the loss of histone H1, which is very important in chromatin organization [8, 11, 25, 35].

In the studies using extracted chromatin, the released chromatin was either kept in the hypotonic buffer that is used to lyse the nuclei or dialyzed into another artificial buffer for further study. Between the native condition inside the nucleus and the *in vitro* artificial buffer, there are many differences that may also cause structural changes of chromatin.

1) a wide range of proteins that can modulate the higher order structure of chromatin exist inside the nucleus but are absent in artificial buffers. For example, ATP-dependent chromatin remodelers are involved in nucleosome disassembly, nucleosome positioning and exchange of canonical histones and histone variants [45, 46]. These chromatin remodelers can alter DNA-histone interaction and regulate chromatin structure at nucleosome level. Some of these remodelers are abundant *in vivo*. It was reported that the ISWI protein, which is the ATPase subunit that marks ISWI chromatin remodelers, was expressed throughout *Drosophila* development at a level of more than

one ISWI molecule every 20 nucleosomes [47]. Another group of proteins that can affect structural dynamics of chromatin *in vivo* is chromatin architectural proteins that can shape the chromatin by binding to DNA. The chromatin architectural proteins have different effects on DNA, such as bending, bridging or wrapping it [48]. Members of the HMG (high mobility group)-box family are important chromatin architectural proteins that exist in abundance (~1 molecule every 10-15 nucleosomes) *in vivo* and can bend DNA substantially to facilitate the assembly of nucleosomes [49]. Proteins in the HMG-box family are highly conserved between species and lack specificity in DNA binding. All of these characters suggest that the HMG-box proteins have a general and basic function in chromatin organization. The abundance of chromatin remodelers and chromatin architectural proteins suggest that they are important in the maintenance and regulation of chromatin structure on both local and global scales in the nucleus. If chromatin structure is studied without these related proteins, the results may go far from the scenario *in vivo*.

2) The total amount of chromatin of one cell is confined into the volume of the nucleus *in vivo* while in *in vitro* system, the chromatin is spread out and highly diluted. For a mammalian cell with a small nucleus, DNA accounts for about 10% (100 mg/ml) of the nuclear mass (including water), which is 500 times higher than the concentration used for *in vitro* experiments (e.g. 200 µg/ml) [50]. This difference in

chromatin concentration can change the interactions between nucleosomes and therefore affect the higher order structure of chromatin;

3) The concentration of divalent ions used in *in vitro* studies (0.2~2 mM) were usually lower than the estimated total concentration of divalent ions in interphase nuclei. Using secondary ion spectrometer analysis, Strick *et al.* measured divalent cation concentration in both interphase and mitotic Indian muntjac deer cells.  $\text{Ca}^{2+}$  and  $\text{Mg}^{2+}$  were the two most abundant divalent cations in nuclei and the total concentration of  $\text{Ca}^{2+}$  and  $\text{Mg}^{2+}$  throughout the whole cell cycle was always much higher than the concentration used in most chromatin structure studies (Table 1) [51]. Thus we classify the buffers used in these *in vitro* studies as a low-salt condition compared with the *in vivo* condition (Figure 6). In a nucleosome, only about 57% of the negative charges of DNA are neutralized by positive residues in the histone octamer, so the remaining charges must be neutralized by other factors like linker histones and cations in the nucleus [52-54]. In low-salt buffer conditions, 10 nm nucleosomal fibers will slightly repel and isolate from each other due to their negative charges [52]. Thus in *in vitro* systems, the chromatin will adopt a swelling conformation due to the low-salt condition.

**Table 1. Ca<sup>2+</sup> and Mg<sup>2+</sup> concentrations in interphase and mitotic cells (adapted from Strick *et al.*, 2001) [51]**

	Ca <sup>2+</sup> (mM)		Mg <sup>2+</sup> (mM)		Total	
	Interphase	Mitosis	Interphase	Mitosis	Interphase	Mitosis
Nuclei	4~6	12~24	2~4	5~17	>6	>17
Entire Cell	7~9	4~8	1~3	12~22	>8	>16

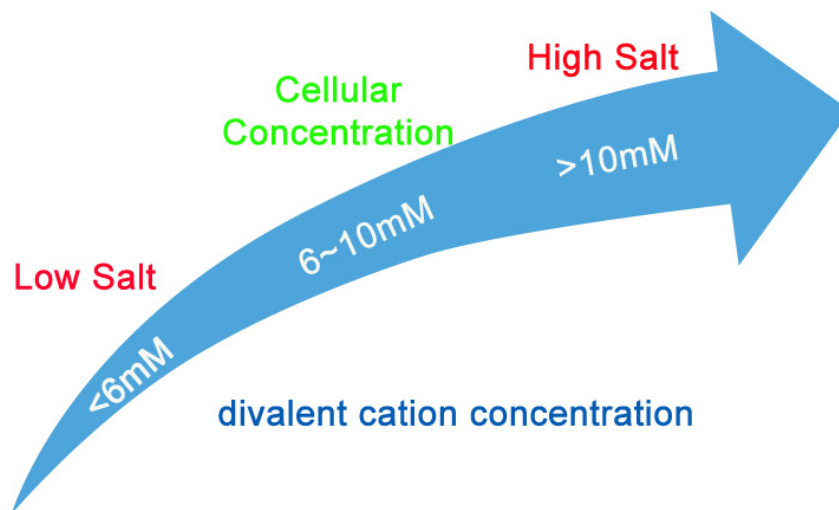


**Figure 6.30 nm chromatin fiber were formed in low-salt conditions.**

As we can see from the above discussion, the chromatin extraction procedures and the *in vitro* study system both can bring a lot of changes to the native chromatin structure. Whether the results from these *in vitro* studies can represent what chromatin looks like *in vivo* remains a question.

### 1.3.2 Evidence from *in situ* experiments

Until now, in all the *in situ* studies of chromatin structure, the 30 nm fiber could only be observed by cryo-EM in two kinds of cells, chicken erythrocytes and marine invertebrate sperm including sperm of sea urchins, sea cucumbers and starfish [14-16]. Both kinds of cells are terminally differentiated cells that have no transcription [55-58]. In chicken erythrocytes, a very basic linker histone H5 exists together with the linker histone H1. During erythropoiesis, the concentration of H5 increases dramatically from 0.2 molecules every nucleosome to ~1 molecule every nucleosome while the concentration of H1 (1 molecule every nucleosome) remains unchanged [59]. Because linker histone was shown to stabilize chromatin folding [8, 60], with linker histone number doubled, chromatin from mature chicken erythrocyte would adopt a more condensed conformation. The post-translational state of H5 is also significantly different from cells from other chicken tissues as well as mammalian cells [61, 62]. In marine invertebrate sperm,  $\phi 1$  histone, which is also a highly basic, lysine-rich histone like H5 in chicken erythrocyte, replaces H1 completely [63, 64]. Chromatin from both chicken erythrocytes and marine invertebrate sperms also has longer nucleosome repeat length than other eukaryotic cells that can carry out transcription normally [59, 65, 66]. All the above characters shared by chicken erythrocytes and marine invertebrate sperm make these two types of cells quite distinguished from other eukaryotic cells.

It is possible that due to the loss of transcriptional ability, chromatin of these two types of cells have adopted a rather special organization form that can hardly represent chromatin organization in other cells with transcriptional activity. Thus, much caution is needed when we interpret results from *in situ* studies using these two kinds of highly specialized cells. The lack of *in situ* evidence from transcriptionally active cells, rather than chicken erythrocytes and marine invertebrate sperms, is the main challenge to the 30 nm chromatin fiber model.

### **1.3.3 Evidence from reconstituted oligonucleosomes**

The DNA sequences used in the reconstitution were originally from sea urchin 5S ribosomal RNA gene or the 601 sequence. The genes coding ribosomal RNA, which are transcribed by RNA polymerase III, have a quite different mechanism of transcription regulation compared with the majority of genes that are transcribed by RNA polymerase II [67, 68]. The 601 sequence was only selected for its higher affinity for histone octamer and precise positioning, thus there is a bias in the DNA-histone interaction at the beginning of the reconstitution and this synthesized sequence doesn't exist in nature. Although the exact effect of DNA sequence on nucleosome organization remains controversial, it is clear that histone have different affinities to different genomic DNA sequences and the differences in histone affinities have an important role in nucleosome organization *in vivo* [69-72]. Using nucleosome

arrays based on one single DNA sequence to simulate the organization state of the whole genome is of high risk to overestimate the influence of one conformation while losing the whole picture and it is more unreliable when this DNA sequence does not even exist in nature.

Furthermore, the histones in the reconstituted oligonucleosomes were either from recombinant *Xenopus laevis* histones expressed in *E.coli* cells or from isolated chicken erythrocytes. The acetylation and phosphorylation level in chicken erythrocyte histones is very low compared with other eukaryotic cells [61, 73] and the recombinant *Xenopus laevis* histones were completely without any post-translational modifications. Post-translational modifications of histones play a very important role in chromatin structure regulation [74, 75]. The structure of the reconstituted nucleosomes using histones from these two sources may mislead us in understanding the mechanisms behind chromatin folding. The highly special features of the selected DNA sequence and histone octamer make the reconstituted nucleosomes unrepresentative of *in vivo* nucleosomes.

#### **1.3.4 Problems with conventional TEM methods**

Due to the size and complexity of chromatin, TEM is the most effective method to study chromatin structure. There are two fundamentally different classes of TEM sample preparation, the



conventional methods and cryo-based approaches [76]. Most of the evidence, both *in vitro* and *in situ*, which contributed to the establishment and the spread of the 30 nm chromatin fiber model, came from TEM samples prepared in the conventional way.

The sample preparation protocol for conventional TEM has several steps of harsh treatment including chemical fixation, alcohol dehydration and heavy metal staining, all of which are liable to cause artifacts to native chromatin structures [77]. There were many examples where the artifacts induced by sample preparation misled even the most experienced eyes. One famous example is the bacterial “mesosome”, which was considered a distinct organelle and was extensively studied by bacterial experts from different groups but turned out to be a fixation artifact [78].

Glutaraldehyde or formaldehyde is mostly used as chemical fixative to preserve structure for conventional EM studies. Most of the studies, including *in vitro* studies (both using extracted chromatin and reconstituted nucleosome arrays) and *in situ* studies, have involved aldehyde fixation in their sample preparation. There are many kinds of artifacts that can be induced by the fixation procedure. The modification of lysine in proteins after glutaraldehyde fixation is probably one of the artifacts that should raise cautions in chromatin structure studies. After the reaction of proteins with glutaraldehyde, the amino analysis of the

fixed samples showed that lysine is the only residue that was significantly changed,  $\epsilon$ -amino group of 50~60% of the lysine residues could react with glutaraldehyde [79-81]. Since lysine residues in histone octamers are very important in neutralizing the negative charges of DNA in chromatin and the change of lysine residues proceeds gradually when the fixation is going on, it's very hard to control to what degree the chromatin structure is affected by this artifact [79, 82]. Aldehyde fixation could also cause shrinkage of some structures and a decrease of pH in the reaction solution. In dehydration procedure, the sample is treated with a series of progressively increasing ethyl alcohol solutions to substitute cellular water. Loss of water may lead to shrinkage of some structures and artifacts from dehydration are largely dependent on the previous fixation procedure [83].

The biggest problem with heavy metal staining in structural study is the obscuration of fine structures. For example, the spikes of B/HK influenza virus were well preserved and could be clearly seen in frozen-hydrated samples while uranyl deposition around the surface of the virus distorted and obscured the spike structures in negatively stained samples (Figure 7). The deposition of the heavy metal molecules doesn't always reveal the structural features faithfully and the internal density variations of the structure cannot be visualized. In chromatin structure studies, this problem becomes more complicated. After heavy

metal staining, the whole chromatin was covered by layers of heavy metal. It is impossible to discern meaningful densities that reflect chromatin structure from meaningless densities caused by random deposition of heavy metal molecules (Figure 8). Thus, the measurement of the dimensions of structural features in heavy metal staining is far from reliable and varies depending on different treatments.

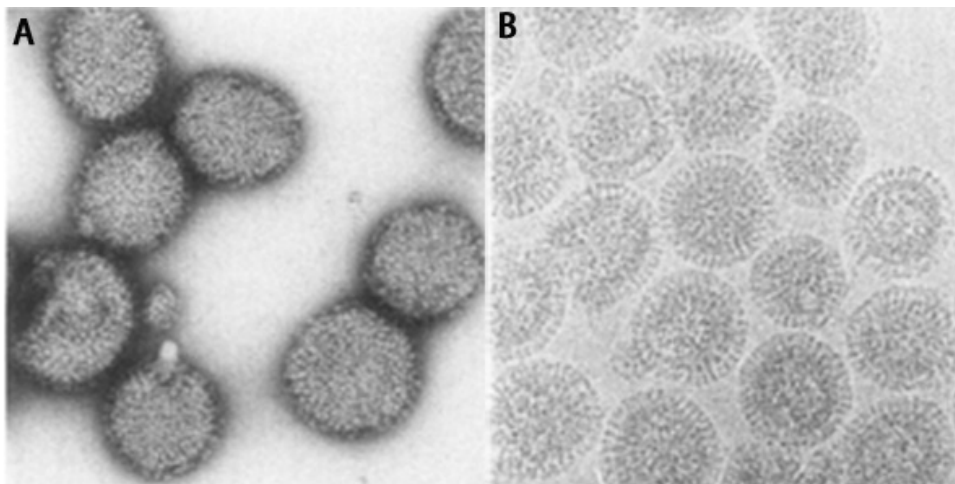


**Figure 7. Obscuration of fine structures by negative staining** (adapted from Booy *et al.*, 1985) [84]. (A) TEM image of B/HK influenza virus negatively stained with uranyl acetate. The spikes of the virus are highly distorted and difficult to resolve. (B) Unstained, frozen-hydrated B/HK influenza virus.

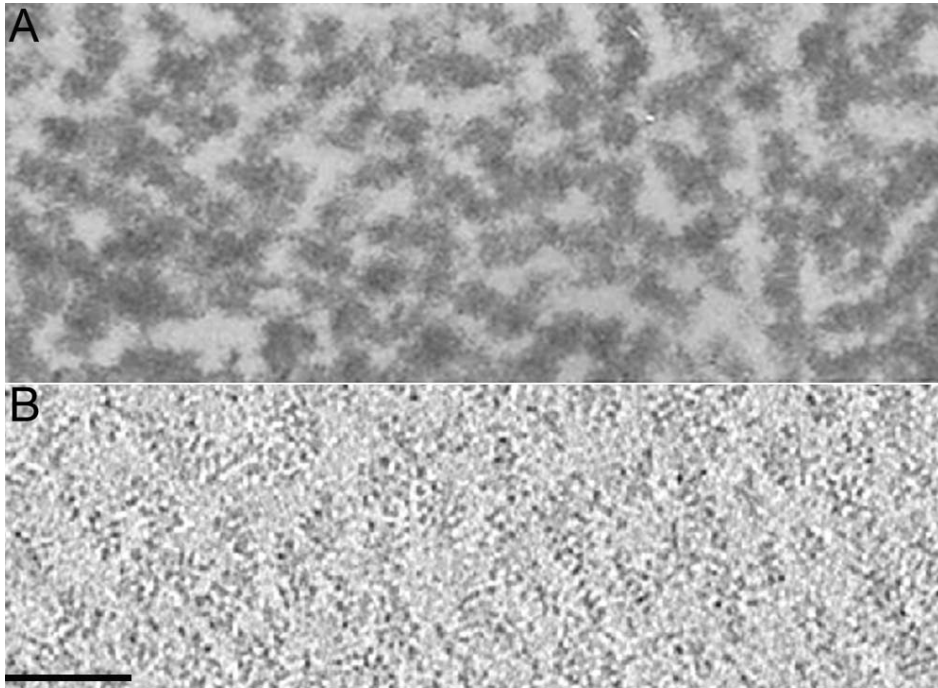


**Figure 8. Comparison of conventional TEM and cryo-EM methods**

(A) TEM image of a 100 nm-thick section of chicken erythrocyte nuclei, glutaraldehyde and osmium tetroxide fixed [85]. The outline of the chromatin fiber was completely covered by the uranyl and osmium molecules. The nucleus was dehydrated and distorted. (B) Cryosection of a chicken erythrocyte nucleus [16]. The nucleus was frozen-hydrated. The structure of the chromatin was well preserved. The resolution was high enough to recognize nucleosome densities. (A) and (B) are of the same scale. Scale bar, 100 nm.

Another problem in chromatin study is that EM images are only 2D projections of samples. The compaction of nucleosomes, no matter *in vivo* or *in vitro*, happens in 3D. From 2D projections, it's impossible to get all the information needed for a correct understanding of chromatin conformation.

From the reexamination of the experimental evidence that support the 30 nm chromatin fiber model, it can be concluded that due to

artifacts from conventional TEM sample preparation, as well as the lack of *in vivo* evidence from most eukaryotic cell types, whether the 30 nm chromatin fiber model really represents a level of chromatin organization inside the cell remains a problem that deserves further investigation. The key to solve this problem is to find a method that will enable us to study chromatin structure *in situ*, to better preserve the native structure of chromatin and to limit imaging artifacts as much as possible.

## **1.4 Cryo-EM in chromatin structural studies**

### **1.4.1 Cryo-EM technique**

The development of cryo-EM makes it possible to observe biological samples in their close-to-native state. Samples are immobilized so rapidly by freezing that water does not have time to crystallize and it remains in a vitreous state with extremely high viscosity [86]. Chemical fixation, dehydration or staining are avoided in sample preparation, thus most of the artifacts that have nagged conventional TEM samples can be avoided. By now, cryo-EM is the “gold standard” to study native structures of biological samples.

Vitrification of a sample can be achieved by plunging the sample into liquid ethane or liquid propane. It is estimated that in plunge-freezing, the freezing rate required is as high as  $10^5 \sim 10^6$  Kelvin/s [76]. For larger samples, high-pressure freezing is used to rapidly cool down the whole sample [87]. Although using high-pressure freezing, samples up to  $\sim 250 \mu\text{m}$  thick can be frozen vitreously, only samples thinner than  $\sim 0.5 \mu\text{m}$  can be imaged directly by TEM [88]. Thick samples must be sectioned before imaging. To cut cryosections, a cryomicrotome is used and it operates below the vitrification temperature. Cryosections as thin as 40 nm can be cut, transferred onto an EM grid and imaged in a cryo-EM [88]. Thanks to plunge-freezing, high-pressure freezing and cryosectioning, in theory any cell now can be imaged in a life-like state.

Single particle analysis and tomography are two ways to study 3D structure of biological samples using cryo-EM. Cryo-EM single particle analysis is mainly used to study 3D structure of molecular assemblies, which are often too large or too flexible to be studied by X-ray crystallography. In single particle analysis, there are multiple isolated copies of the particle (molecule) of interest on the sample grid and the orientations of these copies within the ice layer are different from each other, so their spatial relationships can be described mathematically by a series of rigid-body transformations. When imaged in TEM, projections of such a set of particles are produced. If the angular distribution of these particles is sufficiently uniform, a series of TEM

micrographs, each showing a field with hundreds of particles, will contain all the information needed to reconstruct the 3D structure of the particle [89]. By combining cryo-EM reconstruction of large complex and X-ray structure of each component of the complex, it is possible to get the 3D structure of the assembled complex to near-atomic resolution [90-92]. To reduce image noise and to achieve a near-atomic resolution, the background of the particles should be as clear as possible, so the particles must either be *in vitro* synthesized or purified from their *in vivo* environment and vitrified in a much simpler buffer with as little contamination from other cellular contents as possible. To study 3D structure of macromolecular complexes *in situ* or *in vivo*, in their close-to-native state, however, is by now beyond the power of single particle analysis.

Cryo-ET, on the other hand, is the only way to study subcellular structures *in situ* or *in vivo*. After vitrification, samples are incrementally tilted in TEM through a range up to  $\pm 70^\circ$  and imaged at each step (Figure 9). The whole set of images collected for one sample is called a tilt series. Each image in this tilt series is a projection of the sample from a different angle of view. After alignment and back-projection of the images, a 3D reconstruction or a “tomogram” of the sample can be generated. Because the effective path length through the sample becomes too thick and because the sample holder sometimes can block the electron beam, good images of the sample tilted beyond 60

degrees cannot usually be obtained. There is a wedge-shaped region of data in reciprocal space that is missed. The resolution of the reconstruction in the direction parallel to the electron beam is compromised by this “missing-wedge” artifact. If the tilt series is collected for *in situ* samples, the resolution of the reconstruction will also be decreased by the noisy, crowded background. In general, the resolution of cryo-ET reconstruction cannot reach the resolution of cryo-EM single particle analysis, but its ability to get 3D structural information *in situ* or *in vivo* makes it a valuable tool to study subcellular structures in the context of a cell.

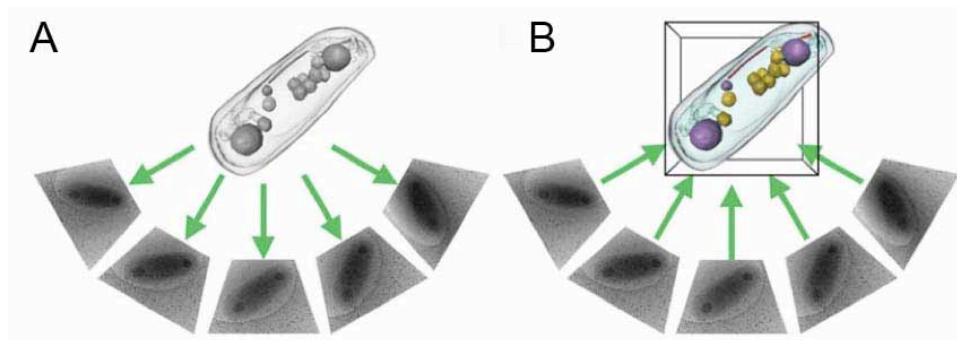


**Figure 9. Summary of cryo-ET (Gan, 2012) [88].** (A) Tilt series of projection images of the sample is collected as the sample is tilted. (B) After 3D reconstruction, a tomogram is generated containing 3D information of the sample.

#### 1.4.2 Cryo-EM in chromatin structure study

Cryo-EM was applied to chromatin structure study almost as soon as the technique was established [93]. With this powerful tool, structural biologists were able to look at chromatin inside cells, without the



artifacts of conventional TEM. However, instead of confirming the textbook model of 30nm chromatin fiber, the results pointed to an opposite direction.

Using Cryo-EM, McDowall *et al.* first observed vitrified sections of mammalian mitotic cells *in situ*, including Chinese hamster ovary cells and HeLa cells, unfixed and unstained [93]. At that time, they only collected 2D projection images of the vitrified sections and found that the mitotic chromosomes were formed by compact association of the 10nm chromatin fiber and that no higher order structure of chromatin inside the cells, including the 30 nm fiber, could be observed. However, in the vitrified sections, ribosomes, which are roughly of the same width as the 30 nm chromatin fiber, and microtubules, which have almost the same diameter and mass per unit length, could be easily identified. The diffraction pattern of the vitrified section did not show any feature that corresponded to 30 nm spacing either. According to these observations, they suggested a liquid model that disorder is equally distributed over the whole chromosome and that local arrangements of nucleosomes could take place without affecting the global organization state of the chromosome.

A study of cryosections of vitrified *Zea mays* meristem cells showed that the condensed chromatin has a grainy texture with a characteristic dimension of 12 nm, which resembled the previously described liquid

model [86]. Bouchet-Marquis *et al.* studied vitrified sections of rat hepatoma, Chinese hamster ovary and Potorus kidney. Similarly, they found that the chromatin appeared to be finely granular and homogeneous. The graininess of the chromatin is of a dimension of 11 nm and there was no discernable structure of larger dimensions [94].

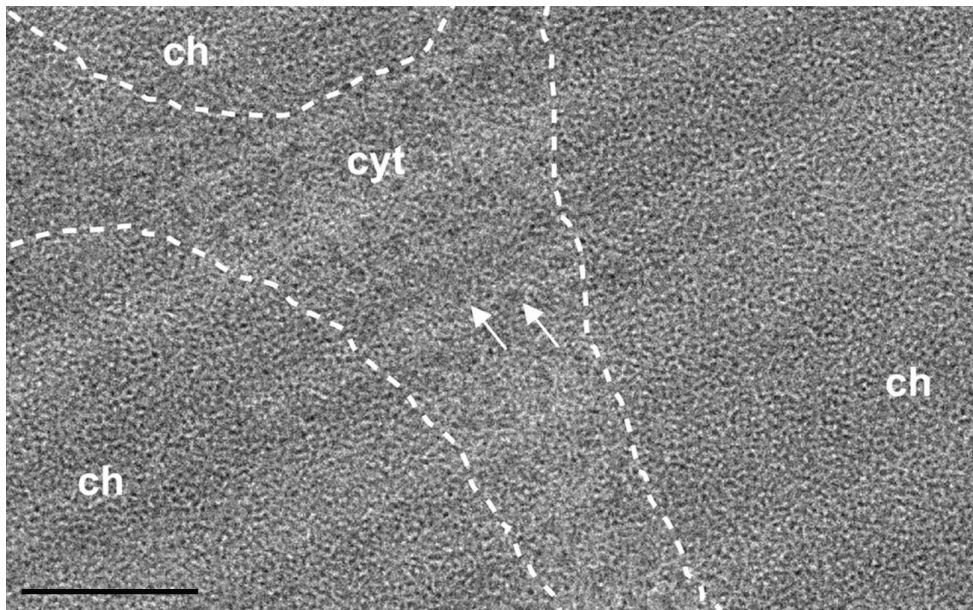


**Figure 10. Cryosection of a HeLa cell (adapted from Eltsov *et al.*, 2011) [95].** The image shows an area of a mitotic HeLa H3 cell cryosection. The 3 parts of chromosomes (ch) are outlined in white and separated by the cytoplasm (cyt). The chromosomes have a homogeneous grainy texture, with no discernible higher order structure. Scale bar, 200 nm.

Another analysis of the 2D projection of a vitreous section from a mitotic HeLa cell by Eltsov *et al.* reached a similar conclusion. 30 nm chromatin fibers were not discernible by visual inspection; 1D rotationally averaged power spectrum analysis of the chromosome images also gave no indication of 30 nm chromatin fibers [95]. Based

on the liquid model, they put forward the polymer melt model to explain the interactions between nucleosomes inside mammalian nucleus (Figure 10, 11).

In the polymer melt model, a nucleus is like a sea of “nucleosomes” (Figure 11). Due to the huge amount of nucleosomes and the small volume of the nucleus, the nucleosome concentration is very high. For example, the average nucleosome concentration in interphase HeLa cells is around 140  $\mu\text{M}$  and can be as high as 250  $\mu\text{M}$  locally [96]. In addition to positive charged histone octamers, the high concentration of cations inside the nucleus further neutralizes the negative charges of DNA and the nucleosomes can be very close to each other. Because of the high condensation, the inter- and intra- 10 nm fiber interactions between nucleosomes cannot be distinguished. Thus, the nucleosomes inside the confined volume of a nucleus are in a uniformly disorganized state and no large-scale higher order structure can be formed either in interphase cells or in mitotic cells.

For extracted or reconstituted chromatin, the nucleosomes are greatly diluted and 10 nm fibers are isolated from each other. The intra-10 nm fiber forces between nucleosomes become dominant. Because the concentration of cations is lower compared to the *in vivo* state, for nucleosomes inside the same 10 nm fiber, the distance between them would increase. Each 10 nm nucleosomal fiber will now compact into a

30 nm chromatin fiber because this is the most stable structure under diluted, low-salt conditions.

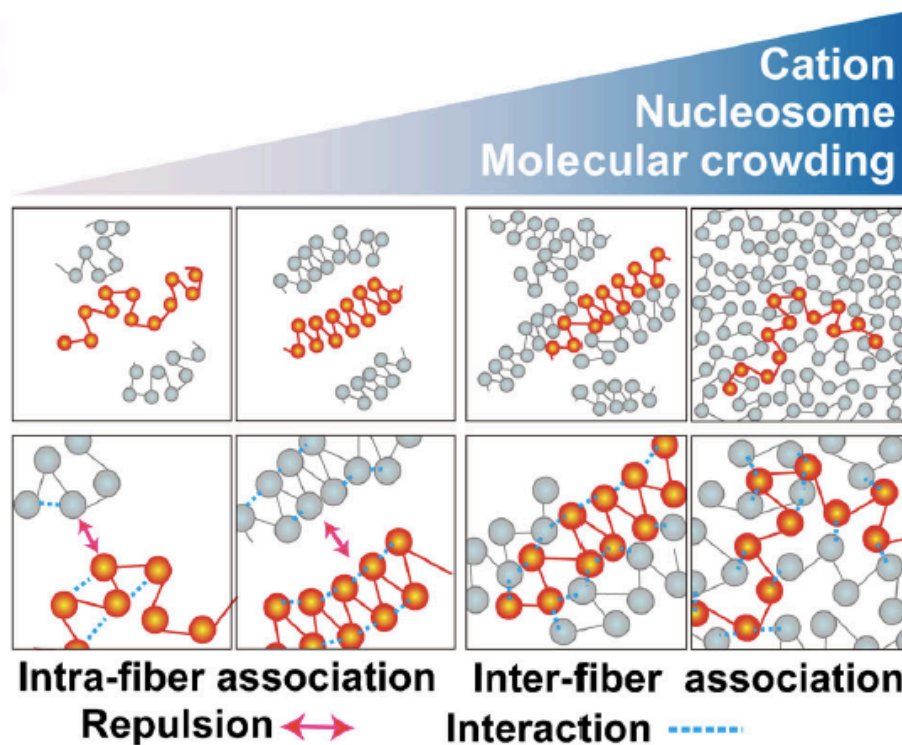


**Figure 11. Polymer melt model (Maeshima *et al.* 2014) [52].**

Under low-salt conditions, nucleosome fibers could form 30 nm fiber structure via intra-fiber nucleosomal interactions. An increase in salt (cation) concentration results in the increase of inter-fiber nucleosomal interaction, leading to a polymer melt scenario. Arrows and dotted lines show repulsion forces and interactions respectively.

If this assumed transition from 10 nm nucleosomal fiber to 30 nm chromatin fiber could be confirmed, the polymer melt model would be able to explain both the presence of the 30 nm chromatin fiber *in vitro* and the absence of the 30 nm fiber *in vivo*.

Now the polymer melt model has become an alternative model to the 30 nm chromatin fiber to describe chromatin organization inside cells

[21, 52]. However, under diluted and low-salt conditions, whether chromatin could convert from the *in vivo* amorphous “sea of nucleosomes” to 30 nm fibers has not been thoroughly tested.

### **1.5 Chromatin study in *Ostreococcus tauri***

*Ostreococcus tauri* (*O. tauri*), first identified in 1994, is a unicellular, marine green alga [97]. It is the smallest known, free-living eukaryote with only one nucleus, mitochondrion, chloroplast and Golgi body (Figure 12). The cell size of *O. tauri* is about 1  $\mu\text{m}$  in diameter. *O. tauri* belongs to the Prasinophyceae lineage, which is an early branch from the green lineage that includes the land plants. Because of its small size and its simplicity in ultrastructure, *O. tauri* has been put forward as a new model organism for study of eukaryotic cells, especially in the area of subcellular structural study. *O. tauri* has 20 linear chromosomes and a genome of 12.56 Mb. 8,166 protein-coding genes were predicted in the genome and 6,256 predicted genes are supported by homology with known genes [98]. The genome size of *O. tauri* is similar to that of the yeasts, *Saccharomyces cerevisiae* and *Schizosaccharomyces pombe*, although the yeasts have much larger cell size. *O. tauri* genome has an extremely high gene density, partly due to reduction of intergenic regions and other forms of gene compaction such as gene fusion and very few repeated sequences. The average intergenic size of *O. tauri* genome is only 196 bp, which is shorter than other eukaryotes with a similar genome size [98]. By

growing *O.tauri* cells in a twelve-light-twelve-dark cycle, the cell cycle can be partially synchronized [99].

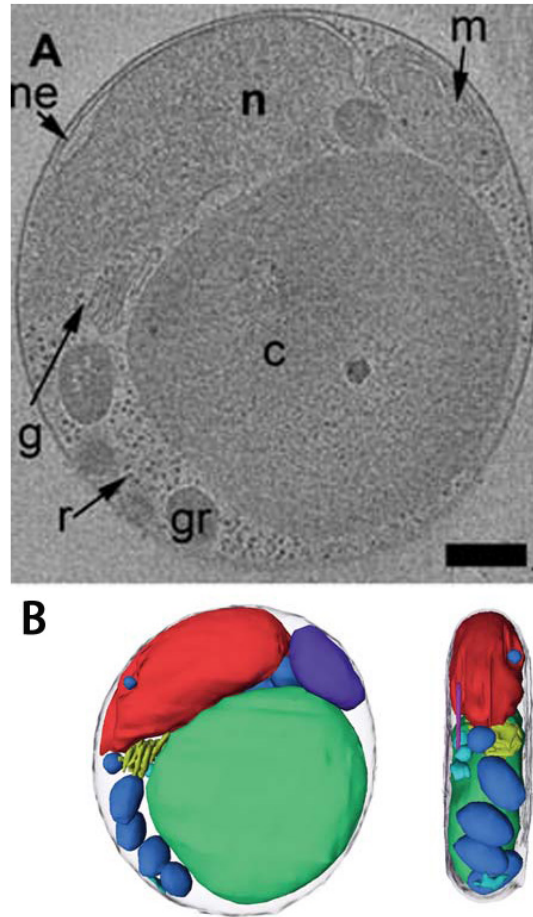


**Figure 12.3D ultrastructure of *O.tauri* (adapted from Henderson *et al.*, 2007)[100].** (A) A 21.6nm central slice of a 3D tomogram of a *O.tauri* cell. (B) A manually segmented model (two perpendicular views) of the same cell. The letters and colors identify nuclei (n, red), nuclear envelope (ne), chloroplasts (c, green), mitochondria (m, dark purple), Golgi bodies (g, yellow), granules (gr, dark blue), inner membranes including ER (light blue), microtubules (light purple), and ribosome-like particles (r). Scale bar, 250 nm.

Because of the limitations for sample thickness by cryo-EM, most cryo-EM studies were carried out mainly on purified macromolecules,

viruses and bacterial cells. Thanks to the tiny size of *O. tauri*, it is now the only eukaryote that can be examined by cryo-EM in a whole cell form [100, 101]. Henderson *et al.* imaged whole cells of *O. tauri* at various stages of the cell cycle by cryo-ET. After reconstruction, they were able to examine the 3D ultrastructure of the whole cell (Figure 12). This work, by characterizing the morphological features of each organelle, paved the way for other cryo-EM studies that also use *O. tauri* as a model organism. Using cryo-ET, Gan *et al.* were able to visualize the chromatin organization of *O. tauri* in both interphase and mitotic cells [101]. They found that unlike higher eukaryotes, *O. tauri* does not undergo large-scale chromatin condensation in mitosis [101]. No higher order structure of *O. tauri* chromatin was found, including the 30 nm fiber. Like HeLa cells and mouse fibroblast cells, the chromatin of *O. tauri* resembles a uniformly distributed “sea” of nucleosomes (Figure 13), which suggested that the polymer melt model better describes chromatin organization of this tiny organism. *O. tauri* is the only non-mammalian cell known to have such a disorganized nucleosome arrangement. The study of *O. tauri* chromatin may give us new insights on the role of chromatin organization in many conserved cellular processes.



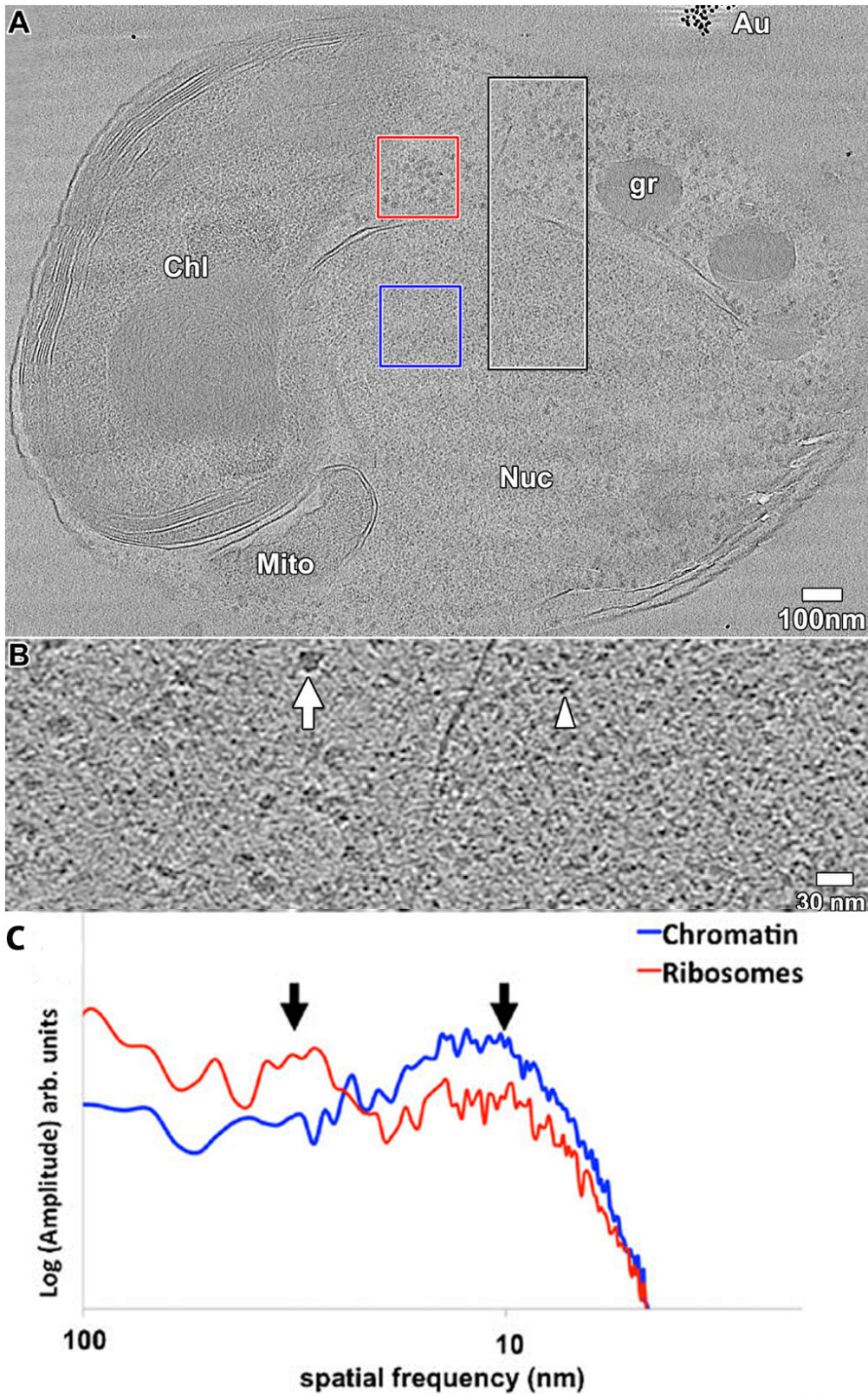


**Figure 13.** *O. tauri* chromatin is not organized as 30 nm fibers (adapted from Gan *et al.*, 2013) [101]. (A) A 60 nm-thick tomographic slice through a cryosection of a mitotic *O. tauri* cell. The nucleus shows a homogeneous



texture where no higher order structure can be identified. Chl, chloroplast; Mito, mitochondrion; Nuc, nucleus; gr, granule; Au, gold fiducials. Chromatin (blue box) and cytoplasmic ribosomes (red box) were selected for Fourier analysis in (C). (B) A 10 nm-thick tomographic slice corresponding to the black/white box in (A). Arrow indicates cytoplasmic ribosome and arrowhead indicates a nucleosome-like density. (C) Rotationally averaged amplitudes (log scale, arbitrary units) of the Fourier transform of the two color-coded positions boxed in (A). Arrows point to the 30 nm (left) and 10 nm (right) spatial frequencies.

In this project, we examined the 3D chromatin organization in *O. tauri in situ* using cryo-ET, without any chemical fixation or staining. (“*In situ*” here means we study chromatin inside lysed cells with all the other cell contents in place. It is different from what we have defined as the “*in vivo*” or “native” state, which is the living cell state.) We have tested whether the diluted nucleosomes can form the 30 nm chromatin structure under low-salt conditions with the presence of  $Mg^{2+}$ . Our results showed that *O. tauri* chromatin, which doesn’t have 30 nm fiber structure *in vivo*[101], could be induced into 30 nm fibers if the chromatin is released from lysed cells in a low-salt buffer with 1 mM  $Mg^{2+}$ .

Results from this project confirmed the transition predicted by the polymer melt model that disordered nucleosomes, which are highly concentrated, could form 30 nm fibers if diluted under low-salt condition with divalent cations. The potential of nucleosomes to form higher order structures indicates that chromatin functions may be regulated through

locally and dynamically conformational changes of nucleosome organization.

## Chapter 2. Materials & Methods

### 2.1 Cell growth and preparation for plunge-freezing

*Ostreococcus tauri* strain OTH95 cells (acquired from the Roscoff Culture Collection) were grown in artificial sea water (ASW) containing Sigma sea salt and Keller enrichment medium (Table 2 and 3), in a twelve-light-twelve-dark cycle. Under this condition, cells were loosely synchronized and almost all cells were at mid-G1 phase at the beginning of the light phase [99]. 50 ml cell culture were harvested in mid-log phase ( $OD_{600} \sim 0.05-0.1$ ) shortly after the dark-to-light transition and pelleted by centrifuging at  $5000\times G$  for 10 minutes at  $4^{\circ}C$ . Cells were then resuspended in 1 ml pre-chilled ( $4^{\circ}C$ ), fresh ASW and pelleted again at  $5000\times G$  for 1 minute. The cell pellet was then resuspended in pre-chilled ( $4^{\circ}C$ ) lysis buffer to make to a final  $OD_{600} \sim 20$ . Treatment of the lysis buffer (from the time point of adding the lysis buffer to the cell pellet to the time point of plunge-freezing) lasted for 10-15 minutes and was carried out on ice. The lysis buffer contained 144 mM sucrose, 6% glycerol, 20 mM HEPES and protease inhibitor cocktail (EDTA-free, Roche, Cat. No. 11836170001). Using a combination of sucrose and glycerol, the concentration of soluble particles (ions and undissociated molecules) in the lysis buffer was adjusted to  $\sim 820$  mM, which is roughly 4/5 of the concentration of

soluble particles in ASW (~1M). Thus, the osmolarity of the lysis buffer should also be about 4/5 of the osmolarity of ASW in simplified estimation if we consider the osmotic coefficient of all the soluble particles to be 1. To induce 30 nm fiber formation, 1 mM Mg<sup>2+</sup> was added to the lysis buffer. As controls, lysis buffer with 0 mM Mg<sup>2+</sup> and lysis buffer with 5 mM EDTA were also used.

**Table 2. ASW composition**

Contents		Concentration
Sea salt		37g/L
F/2 vitamins	cyanocobalamin	0.369nM
	biotin	2.05nM
	Thiamin-HCl	296nM
K trace metal	Na <sub>2</sub> Mo <sub>4</sub> •2H <sub>2</sub> O	26.0nM
	ZnSO <sub>4</sub> •7H <sub>2</sub> O	76.5nM
	CoCl <sub>2</sub> 6H <sub>2</sub> O	42.0nM
	MnCl <sub>2</sub> •4H <sub>2</sub> O	910nM
	CuSO <sub>4</sub> •5H <sub>2</sub> O	39.2M
K medium	NaNO <sub>3</sub>	882μM
	NH <sub>4</sub> Cl	50.1μM
	Disodium β-glycerophosphate pentahydrate	10μM
	H <sub>2</sub> SeO <sub>3</sub>	10nM

**Table 3. Sea salt composition**

Contents	Concentration in ASW
NaCl	41mM
KCl	10mM
MgCl <sub>2</sub> •6H <sub>2</sub> O	20mM
CaCl <sub>2</sub> •2H <sub>2</sub> O	1mM
MgSO <sub>4</sub> •7H <sub>2</sub> O	25mM
NaHCO <sub>3</sub>	2.5mM

## 2.2 Plunge-freezing

Colloidal gold (20 nm, BBI solutions, Cat. No. EM GC20) was washed with 10 mg/ml BSA by first pelleting at 18,000xg for 5 min and then removing the supernatant. The gold was washed twice in this way. The BSA-treated gold was then added to the cells just before plunge-freezing. 3 µl treated cells were added to each side of a plasma-cleaned grid (CF-4/2-2C-T, Protochips). The grids were blotted with filter paper (Grade1, Whatman) for 1 s and then plunge-frozen in 67/33 (% v/v) liquid propane/ethane mixture[102] using a Vitrobot automated plunge freezer (Mark IV, FEI). The relative humidity in the sample chamber of the Vitrobot was kept at 100%. The grids were then stored in liquid nitrogen until use.

### 2.3 Cryo-ET and image processing

For *O. tauri* cells plunge-frozen in lysis buffer with 1 mM Mg<sup>2+</sup>, the grids were loaded into a cryoholder and imaged in a 120 KV, Tecnai 12 transmission electron microscope (FEI). For *O. tauri* cells plunge-frozen in lysis buffer without Mg<sup>2+</sup> or in lysis buffer with 5 mM EDTA, the grids were imaged in a 300 KV, Titan Krios cryo electron microscope (FEI) (see Table 4 for detailed information). Tilt series were collected automatically using Legion software packages [103] in 1° or 2° increment from -60° to +60°. The total dose for each tilt series was 120~150 e<sup>-</sup>/Å<sup>2</sup>.

Using the IMOD software package[104], images were aligned with the help of gold fiducials and the 3D reconstructions were calculated and examined. In reconstruction, boundary models were created using whole tomograms instead of sample tomograms for all samples. For samples treated with 0 mM Mg<sup>2+</sup> and samples treated with 5 mM EDTA, tilt series were first CTF corrected and then 2D low-pass filtered with the cut off and sigma value setting to 0.2 and 0.05 in IMOD. Other parameters remained the default values as set by IMOD.

**Table 4. Electron Tomography Parameters for *O.tauri* cells treated with 1 mM Mg<sup>2+</sup>, 0 mM Mg<sup>2+</sup> and 5 mM EDTA.**

	1mM Mg <sup>2+</sup>	0mM Mg <sup>2+</sup> & 5mM EDTA
Instrument	FEI T12	FEI Titan Krios
Gun type	LaB <sub>6</sub>	FEG
Gun voltage	120kV	300kV
Temperature	80K (liquid-N <sub>2</sub> cooled)	
Tomography package	Leginon	
Nominal magnification	6,500	8,700
Specimen-level pixel	1.428nm	0.895nm
Defocus	-14μm	
Total Dose	120e <sup>-</sup> /Å <sup>2</sup>	150e <sup>-</sup> /Å <sup>2</sup>
Tilt range	±60°	
Tilt increment	1°	1° or 2°
Tilt method	Single-axis	
Dose scheme	1/cosine	
Camera	Gatan UltraScan	FEI Falcon II
Bin factor	2	1
IMOD version	4.5.7	4.7.10

## **Chapter 3. Results and discussion**

### **3.1 Induced 30 nm chromatin fiber**

To induce the 30 nm chromatin fiber, we needed to identify the conditions that allow the intra-10 nm fiber interactions become the dominant interaction between nucleosomes. According to the polymer melt model, we proposed that a low concentration of divalent cations (low-salt condition) and the diluted chromatin are two of the most essential conditions to form the 30 nm fiber. To dilute chromatin from the native concentration inside the nucleus, we disrupted the cell membrane as well as the nuclear envelope by a hypotonic shock using a lysis buffer. Once the cell membrane and nuclear envelope were disrupted, the chromatin was no longer confined to a small volume and was able to distribute over a larger space, which meant that the chromatin was in a diluted condition compared with its native state in an intact cell (Figure 14). However, we wanted to avoid too much perturbation to the cell, because we needed to maintain morphological features of the chloroplast as references to locate the nucleus and the chromatin.



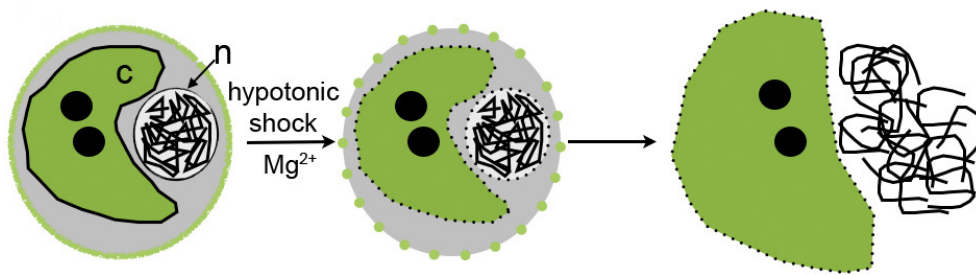


### Figure 14. Steps to induce 30 nm chromatin fiber in *O. tauri*

The lysis buffer will disrupt the cell membrane and nuclear envelope by hypotonic shock while establishing a low-salt condition with 1 mM Mg<sup>2+</sup> for the chromatin. “c” and “n” indicate chloroplast and nucleus respectively.

In *O. tauri*, the chloroplast and the nucleus are the 2 largest organelles and they always reside in opposing halves of the cell (Figure 12 and 13A) [100]. The chloroplast was easy to locate for its biggest size among all the organelles, thylakoid membrane system and two classes of granules inside the chloroplast. Each chloroplast has multiple dark granules and a single granule that is very sensitive to electron beam damage. These granules were the most obvious markers for the chloroplast in TEM images. Due to the simplicity of the ultrastructure of *O. tauri*, once the chloroplast was located, the nucleus could be easily found.

Once the cell membrane was disrupted, the chromatin was suspended in the lysis buffer. Previous *in vitro* studies using buffers containing 0.2 to 2 mM Mg<sup>2+</sup> could observe the formation of the 30 nm fiber structure [7, 8, 29, 105]. Thus, we adjusted Mg<sup>2+</sup> concentration in

the lysis buffer to 1 mM to provide a supportive condition to form the 30 nm fiber structure.

Due to the disruption of the cell membrane by the hypotonic lysis buffer, the cellular contents of *O. tauri* spread over a larger volume compared to intact cells. The following blotting procedure prior to plunge-freezing further flattened the cell. We plunge-froze the cells and directly imaged them in a cryo-TEM. Because *O. tauri* is so small, after hypotonic shock and plunge-freezing, the samples were already thin enough that we could resolve nucleosome-size particles in the final tomograms without cryosectioning. Using cryo-ET, we were able to avoid the artifacts from chemical fixation, heavy metal staining and dehydration and we were able to get 3D information of chromatin organization of *O. tauri in situ*. The lysed *O. tauri* cells prepared using our method were highly reproducible (Figure 15). We also compared our experiments with previous *in vivo* cryo-EM studies of *O. tauri* chromatin in which 30nm fiber structure was absent [101]. Together, this *O. tauri* system revealed the transition of chromatin from *in vivo* polymer melt structure to the 30nm fiber structure.

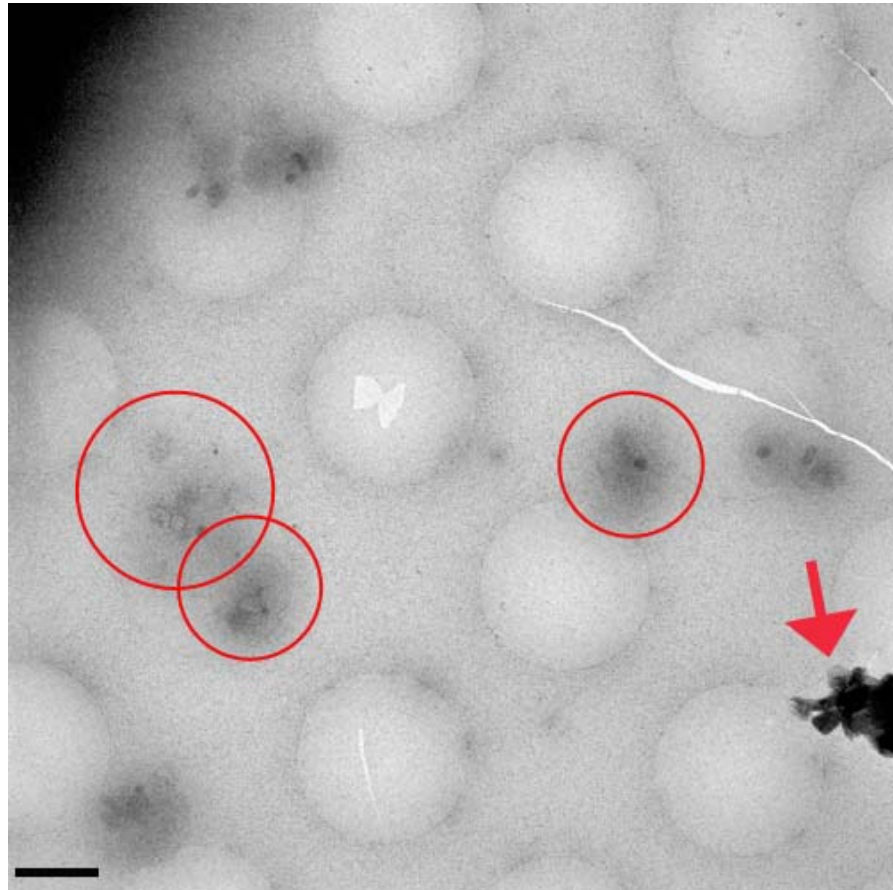


**Figure 15. Low-magnification cryo-EM image of lysed, frozen-hydrated *O. tauri* cells.** The cellular contents of each cell remained together and the overall appearances of different cells were consistent. Red circles indicate examples of lysed cells. The black region marked by the red arrow is an ice contaminant. Scale bar, 2  $\mu\text{m}$ .

### 3.2 Identification of *O. tauri* nucleus

For the identification of *O. tauri* nucleus, the osmolarity of the lysis buffer cannot be too low to make the cell completely lyse. We used a combination of sucrose and glycerol to adjust the osmolarity of the lysis buffer to  $\sim 4/5$  of the osmolarity of ASW to create a slightly hypotonic condition for *O. tauri* cells. Under our experimental conditions, the *O.*

*tauri* cell membrane and nuclear envelope were only partially disrupted. All cellular contents, including the chromatin, distributed over a much larger volume compared to unperturbed *O. tauri* cells (Figure 16, A and B). In most cells, relative location of the chloroplast and the nucleus was preserved so we were able to identify the nucleus in a lysed cell (Figure 16). Although positions and sizes of different organelles varied slightly from cell to cell, the overall appearances of the lysed cells were of high consistency (Figure 17).

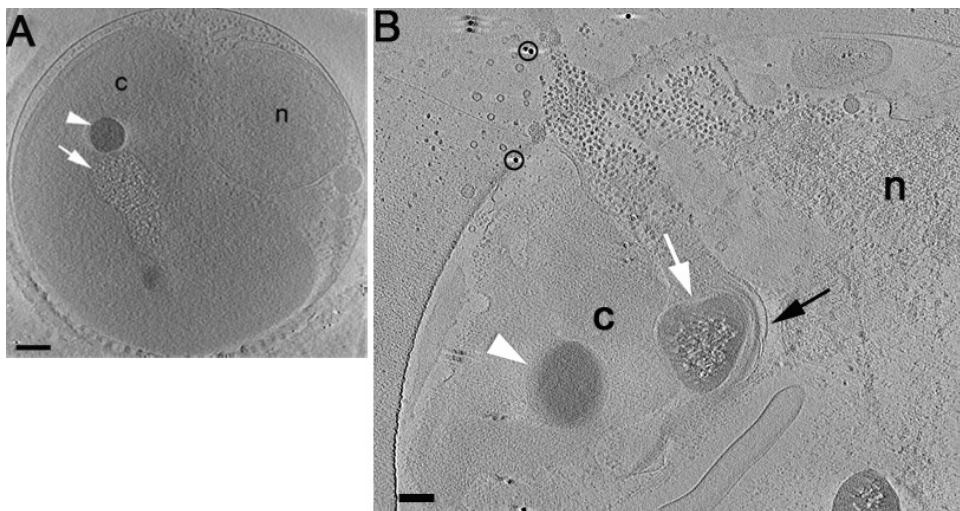


**Figure 16. Identification of *O. tauri* nucleus.** (A) A 24 nm tomographic slice showing intact *O. tauri* cell [100]. The white arrowhead shows the dark granule in the chloroplast and the white arrow shows the granule in the chloroplast sensitive to electron beam damage. “c” and “n” indicate chloroplast and nucleus respectively. (B) A 28 nm tomographic slice of *O. tauri* cell lysed by our lysis buffer. The chloroplast is still identifiable from its thylakoid membranes (black arrow). Densities marked by black circles are representatives of gold fiducials added to the sample to facilitate 3D reconstruction. Note how the lysed cell is spread out laterally and therefore a much thinner sample than the intact cell. Scale bar, 200 nm.

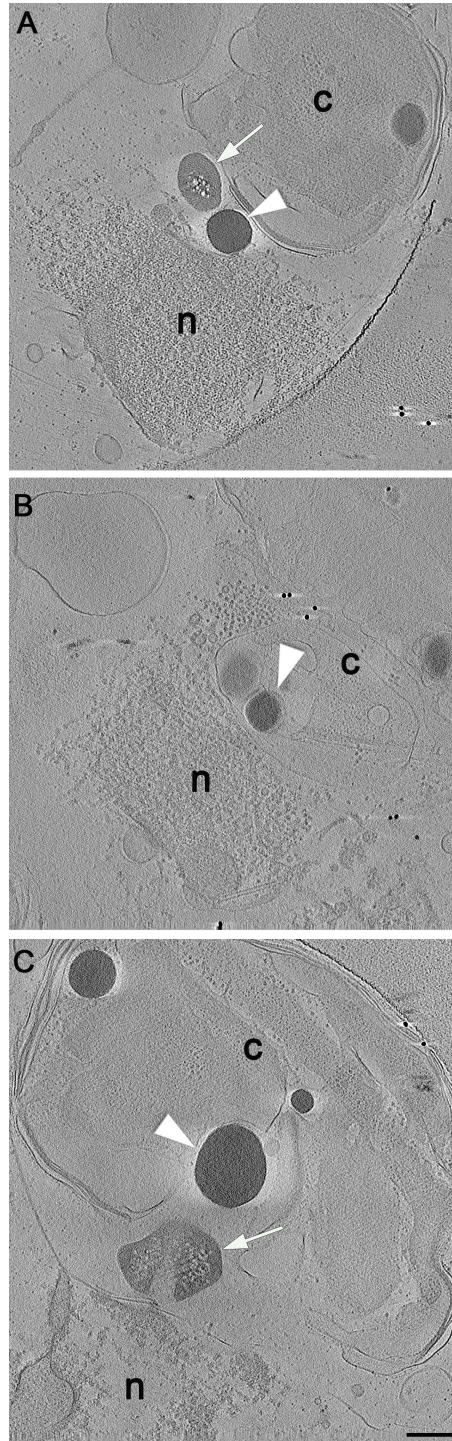


**Figure 17.28 nm tomographic slices of partially lysed *O. tauri* cells treated with 1 mM  $Mg^{2+}$ .** (A-C) Cells are lysed by lysis buffer with 1 mM  $Mg^{2+}$ . Chloroplasts and nuclei are identifiable in all three cells. Scale bar, 200 nm. White arrowheads show the dark granules in the chloroplast and white arrows show the big granules in the chloroplast sensitive to electron beam damage. “c” and “n” indicate chloroplast and nucleus respectively.

### 3.3 Formation of the 30 nm chromatin fiber with 1mM Mg<sup>2+</sup>

In those less perturbed cells, the chromatin was only slightly diluted. Under this condition, individual 10 nm chromatin fiber was not isolated from each other and no higher order structure of the chromatin, including the 30 nm fiber structure, could be found in the tomogram (Figure 18). While in cells that were more perturbed by the hypotonic shock, chromatin would spread to a much larger radius compared with chromatin in an intact nucleus and 30 nm chromatin fibers could be identified in the tomogram after 3D reconstruction (Figure 19). The 30 nm chromatin fibers in these cells, however, could only be observed in the periphery area of the chromatin mass, where some of the 10 nm nucleosomal fibers were isolated from the main body of chromatin mass. Thus, under our low-salt conditions, if *O. tauri* nucleosomes were diluted enough, the 30 nm chromatin fiber could be induced.

The formation of the 30 nm chromatin fiber in our lysed *O. tauri* system raised the question on the role of H1 histone in chromatin compaction. Genome-wide study of *O. tauri* nucleosome positioning suggested that *O. tauri* does not have H1 histone in its chromatin [98]. If this is true, that means nucleosomes have the ability to fold into higher-order structure without linker histones, but perhaps the fibers formed without the presence of linker histones could not be so compact as fibers formed with linker histones. This conclusion would be



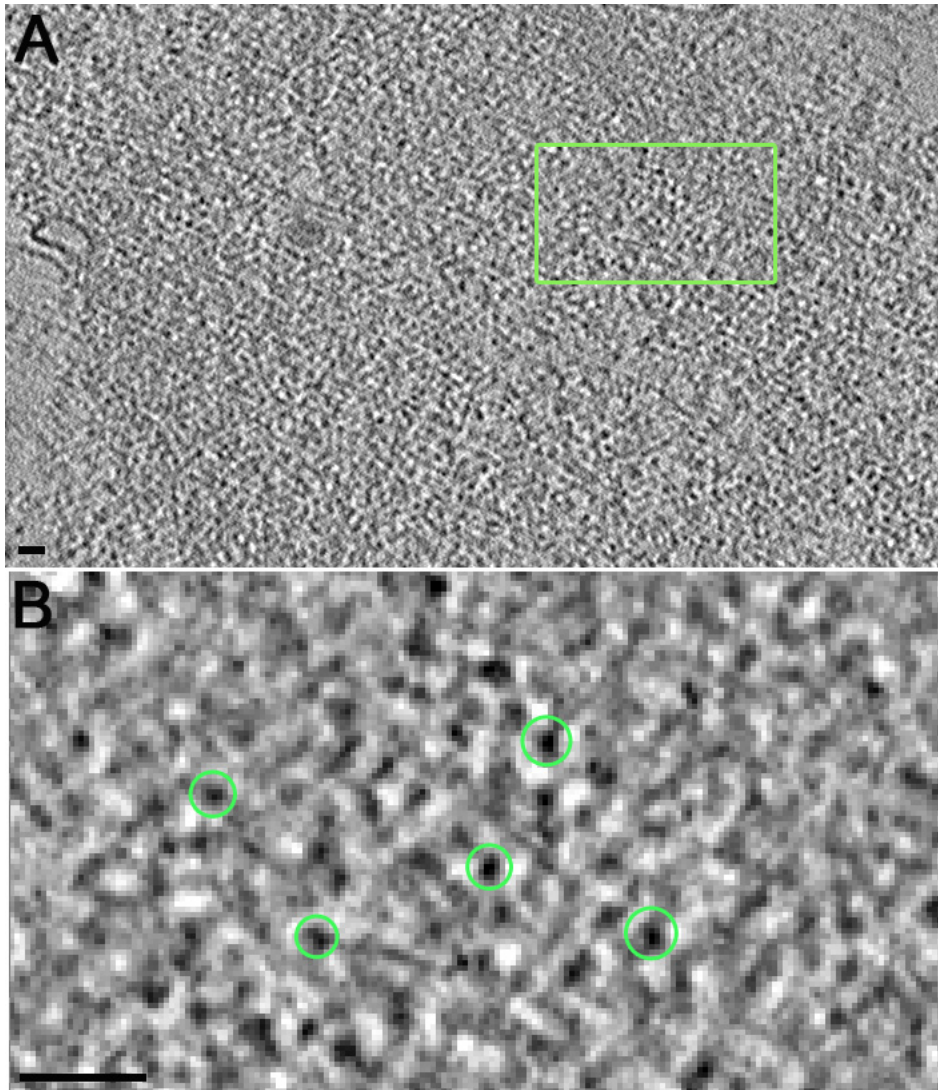


**Figure 18. Polymer melt state of nucleosomes in lysed *O. tauri* cells treated with 1 mM  $Mg^{2+}$ .** (A) 28 nm tomographic slice of the nucleus region from the cell in (Figure 17A). The chromatin was only slightly diluted and no obvious feature resembling a 30 nm fiber structure could be identified. The chromatin remains in a polymer melt state. (B) Enlarged view of the area enclosed by the green box in (A). Nucleosome-like densities can be resolved. Green circles indicate examples of nucleosome-like densities. Scale bar, 100 nm.

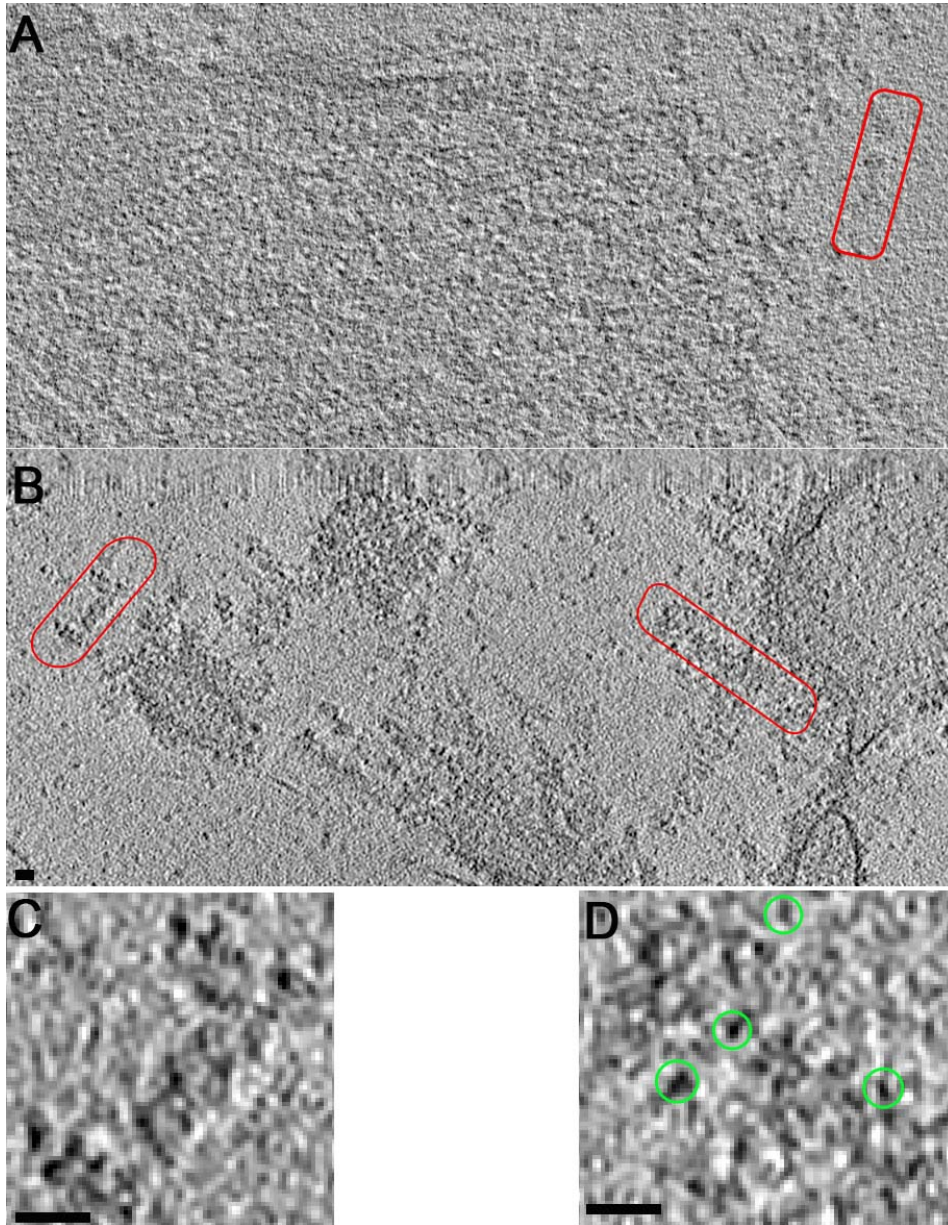


**Figure 19. Formation of 30 nm chromatin fiber in lysed *O. tauri* cells treated with 1 mM  $Mg^{2+}$ .** (A) 28 nm tomographic slice of the nucleus region from the cell in Figure 17B. Nucleosomes were more diluted. 30 nm fiber structures were induced and could be identified. Red ovals indicate the induced 30 nm fiber structures. (B) 28 nm tomographic slice of the nucleus region from the cell in Figure 17C. Nucleosomes were diluted enough to form 30 nm fibers that could be easily identified. (C-D) Enlarged views of the fibers indicated by the red ovals in (B). Green circles indicate examples of nucleosome-like densities. Scale bar, 30 nm.



contradictory to the results from earlier studies that have stressed the necessity of linker histone in the formation of chromatin higher order structures [8, 36]. However, it is also possible that *O. tauri* does have linker histone to facilitate the chromatin compaction which has been observed in our experiments. Once the existence or absence of linker histone in *O. tauri* is confirmed, we will have a better understanding of the role of linker histone in chromatin compaction.

### **3.4 30 nm chromatin fiber could be maintained without external $Mg^{2+}$**

To examine the effect of divalent cations on the formation of 30 nm chromatin fiber structure, we treated the cells with lysis buffer without  $Mg^{2+}$ . Chromatin was clearly more spread out (Figure 20, A and B). However, for most of our samples treated without  $Mg^{2+}$  in the lysis buffer, 30 nm chromatin fiber structures remained one of the major forms of chromatin conformation (Figure 20). This result was quite different from previous *in vitro* studies, in which extracted or reconstituted chromatin was resuspended in artificial buffers with or without divalent cations. In those studies, external  $Mg^{2+}$  provided by artificial buffers was said to mimic physiological conditions and was shown to be essential to the formation of 30 nm chromatin fibers. Without external  $Mg^{2+}$ , most of the extracted or reconstituted chromatin would decondense [8].

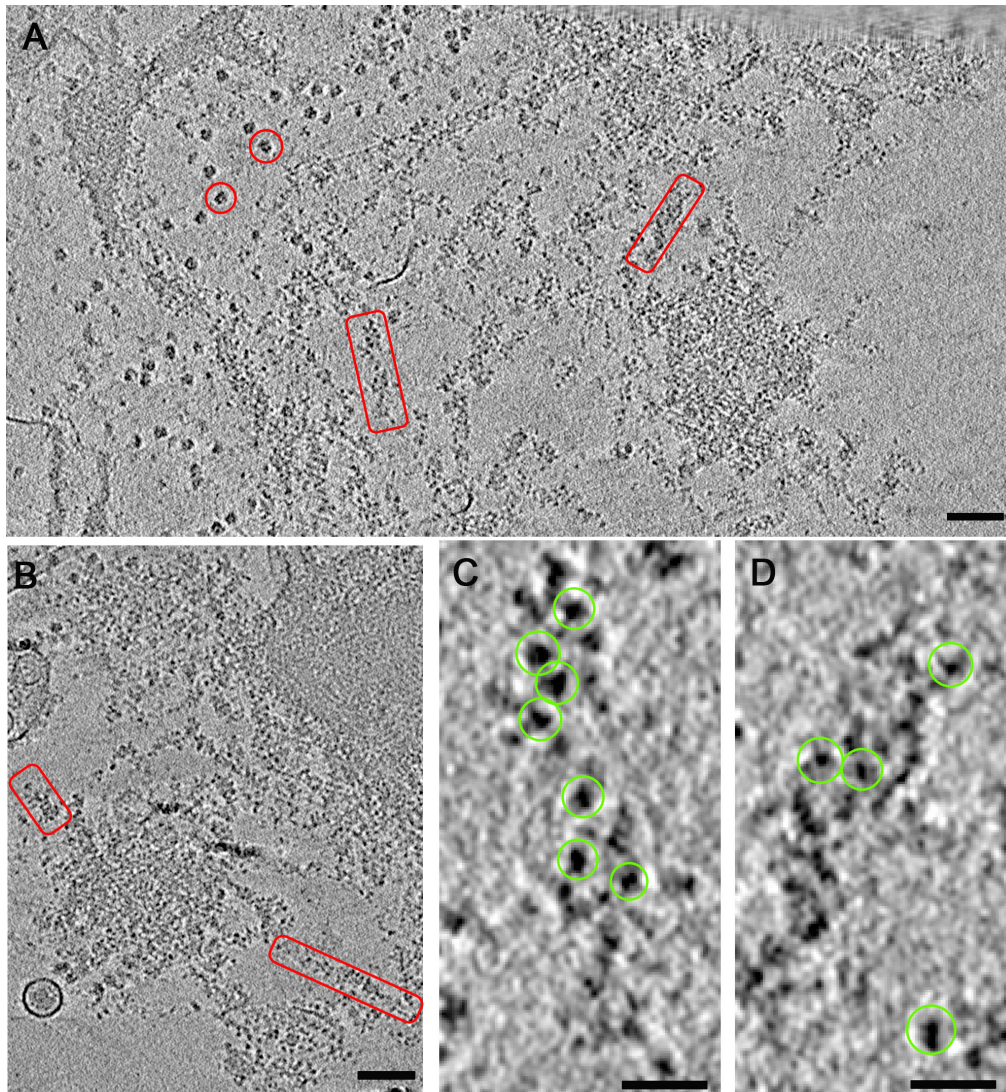


**Figure 20.30 30 nm chromatin fibers were maintained in lysed *O. tauri* cells without external  $Mg^{2+}$ .** (A-B) 28 nm tomographic slice of chromatin region from lysed *O. tauri* cells treated with 0 mM  $Mg^{2+}$  in the lysis buffer. Red ovals indicate the induced 30 nm fiber structures. Red circles indicate examples of ribosomes, which are ~25 nm in diameter and are important internal scale bars. Scale bar, 100 nm. (C-D) Enlarged views of the 30 nm fibers indicated by the red ovals in (A). Green circles indicate examples of nucleosome-like densities. Scale bar, 30 nm.

One possible explanation is that in our experiments, divalent cations (mainly  $Ca^{2+}$  and  $Mg^{2+}$ ), which bind to chromatin *in vivo*, remained bound after cell lysis. These divalent cations could have prevented the

chromatin from complete decondensation in our lysed cells. For extracted chromatin, multiple-step purification could have stripped the chromatin of its *in vivo* binding cations; and for reconstituted chromatin, the only source of cations was the artificial buffer it was suspended in [31, 38]. If this explanation is true, it means that *in vivo*, the binding of chromatin and cations within the same 10 nm nucleosomal fiber is very tight. Alternatively, it is also possible that this binding is protected by other forces like hydration force, which is a force caused by reconfiguration of water between macromolecular surfaces [106]. Whichever was the reason, our lysis treatment with 0 mM  $Mg^{2+}$  was only able to significantly affect the interacting forces between different 10 nm nucleosomal fibers, resulting in the isolation of these 10 nm fibers and then promoting the formation of 30 nm chromatin fiber. The tight chromatin-cation binding revealed in our experiments implied that it could provide one of the major attractive forces between nucleosomes intra-10 nm fiber *in vivo*.

### **3.5 Decondensation of chromatin in 5mM EDTA**

To completely remove divalent cations from *O. tauri* chromatin, cells were treated in our lysis buffer with 5 mM EDTA. Nucleosomes were further diluted and most of the compact 30 nm fiber structures were completely decondensed to linear, 10 nm nucleosomal fibers. The “beads-on-a-string” conformation of the 10 nm fiber could be easily

resolved (Figure 21-23), which supported that the densities we observed were from chromatin. There were still partially decondensed 30 nm chromatin fibers (Figure 21 and 24). In both linear, 10 nm fibers and partially decondensed 30nm fibers, linker DNA densities between two nucleosomes could be detected (Figure 22-24).

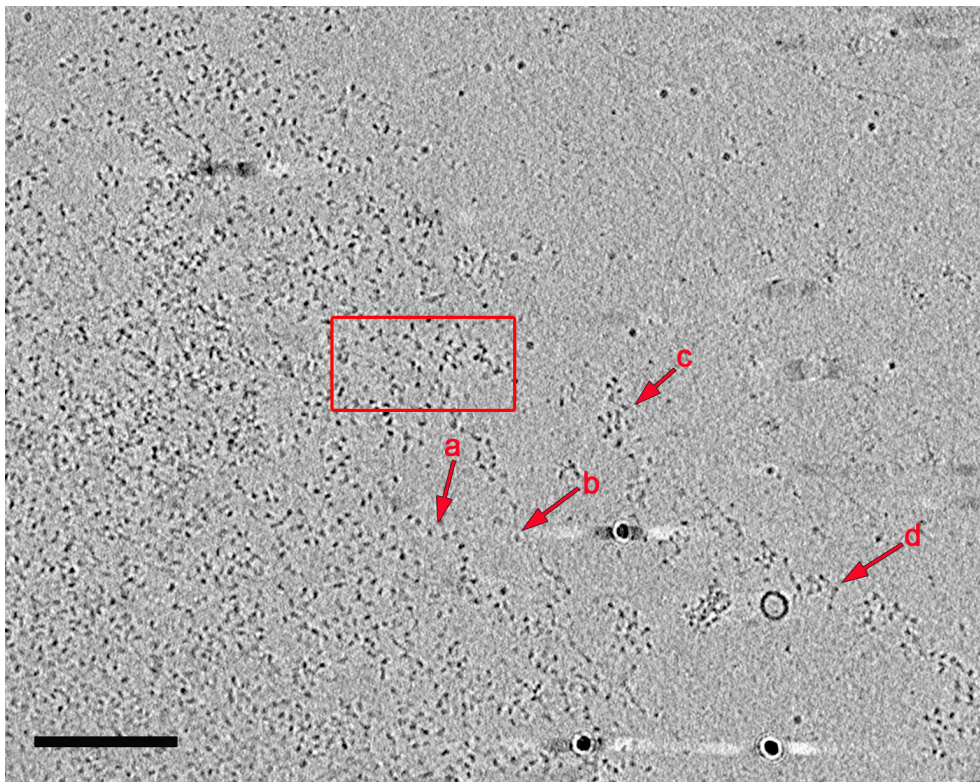


**Figure 21. Decondensed chromatin of lysed *O. tauri* cells treated with 5 mM EDTA.** 28 nm tomographic slice of chromatin region from lysed *O. tauri* cells treated with 5 mM EDTA in the lysis buffer. Scale bar, 200 nm. Arrow a and arrow b indicate completely decondensed chromatin; arrow c and arrow d indicate partially decondensed 30 nm chromatin fiber. Enlarged view of features marked by red rectangle and red arrow a-c are shown in Figure 22- 24.



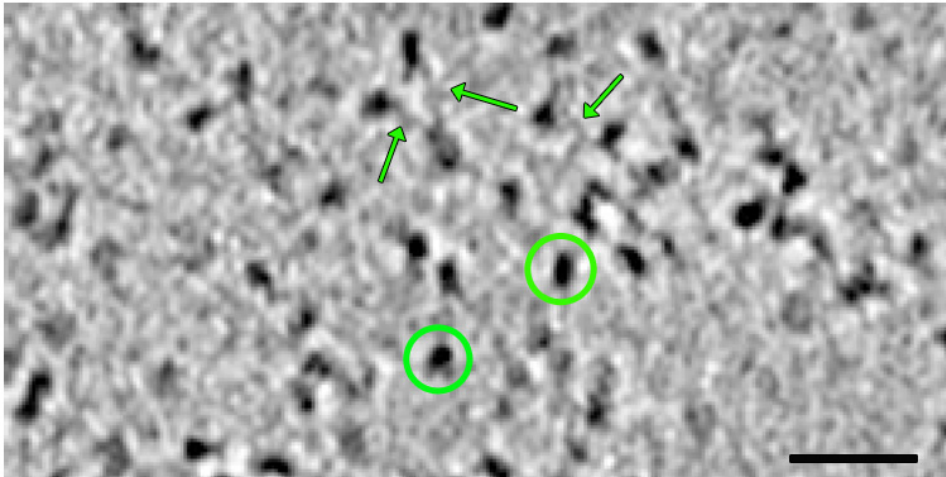


**Figure 22. Nucleosome densities from decondensed chromatin.**

Enlarged view of the area marked by the red rectangle in Figure 21. Green circles indicate nucleosome densities. Green arrows indicate densities from linker DNA between nucleosomes. Scale bar, 30 nm.

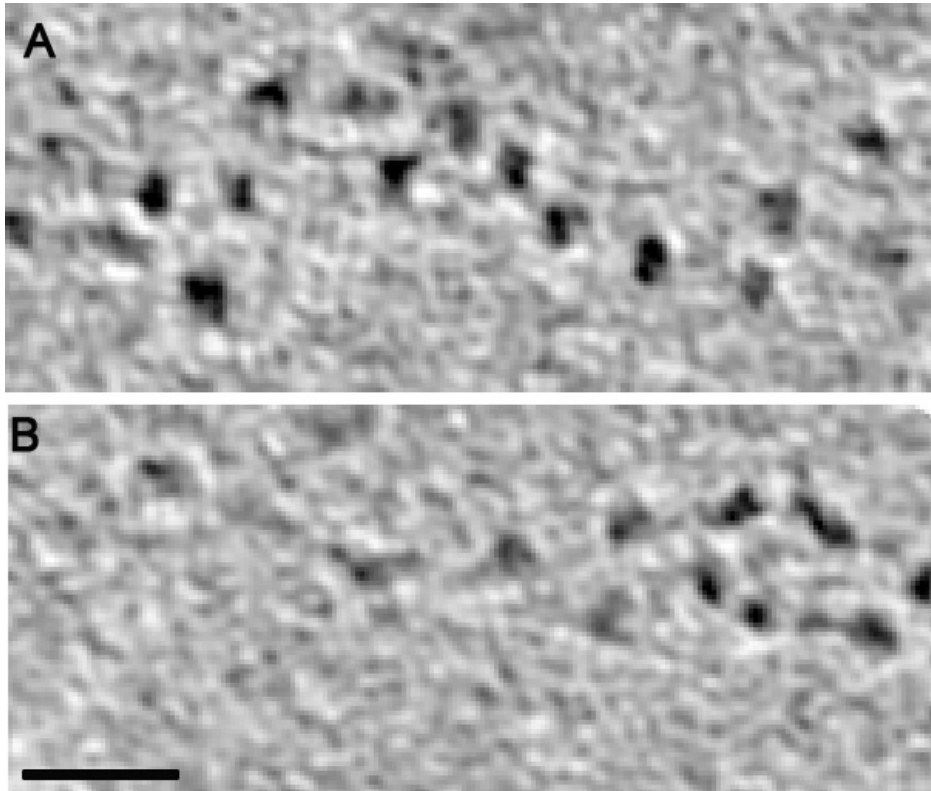


**Figure 23.10 nm nucleosomal fibers in lysed *O. tauri* cells treated with 5 mM EDTA.** (A-B) enlarged view of decondensed chromatin marked by arrow a and arrow b in Figure 21. The 10 nm “beads-on-a-string” structure could be clearly seen. The fibers were rotated  $\sim 135^\circ$  clockwise from their original orientation in Figure 21. Scale bar, 30 nm.

Decondensation of 30 nm chromatin fibers in 5 mM EDTA treated cells supported our conclusion that the maintenance of the 30 nm chromatin fibers in 0 mM  $Mg^{2+}$  treatment was due to residual chromatin-bound cations from *in vivo* state and that these chromatin-binding cations provide the major attractive force between nucleosomes intra-10 nm fiber. After chelating bound cations from the chromatin by EDTA, the repulsive force between neighboring nucleosomes push them away from each other and the compact 30 nm

fiber was decondensed. Partially decondensed 30 nm chromatin fibers in our experiments adopted a conformation that was very similar to the zigzag model [11]. The twisted, zigzag path of linker DNA could be clearly resolved (Figure 24).

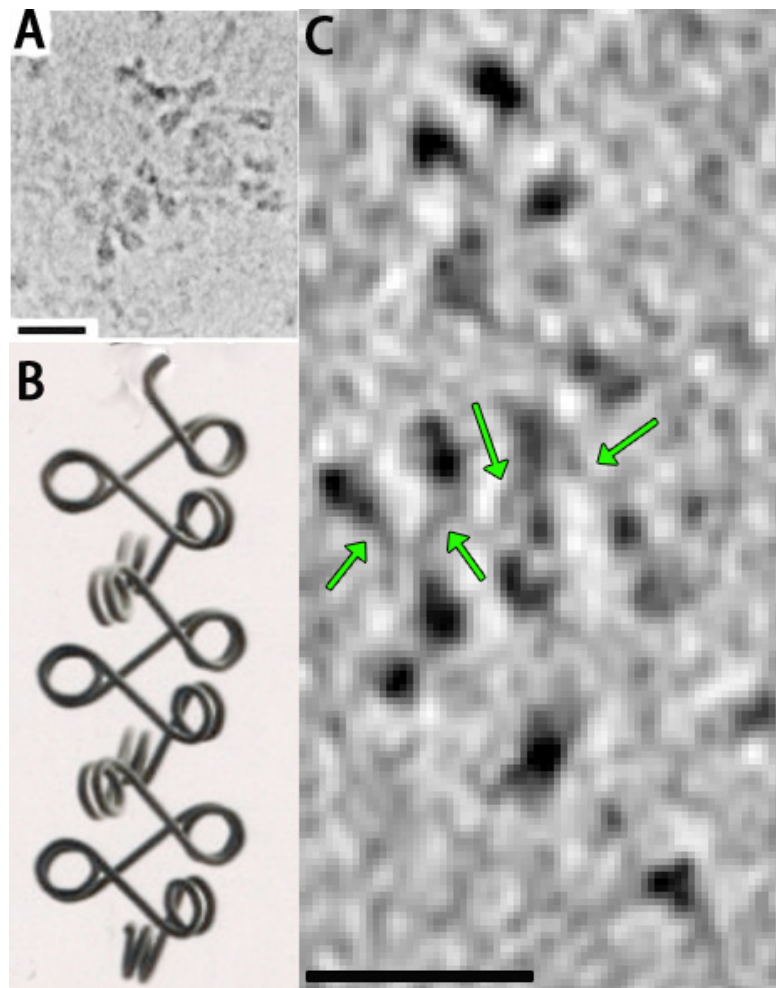


**Figure 24. Partially decondensed 30 nm chromatin fiber in 5 mM EDTA.** (A-B) Zigzag conformation of 30 nm chromatin fiber revealed by previous study using extracted chromatin from COS-7 cells (See Figure 3)[17]. Scale bar, 30 nm. (C) Enlarged view of partially decondensed 30 nm chromatin fiber marked by arrow c in Figure 21. The putative zigzag path of linker DNA was marked by green arrows. Scale bar, 30 nm.

### 3.6 Polymer melt model of *O. tauri* chromatin

Previous *in vivo* studies on *O. tauri* chromatin showed that inside the nucleus the nucleosomes were in a disordered state and formed no higher order structure, resembling the description on chromatin organization from the polymer melt model [101]. Our new experiments confirmed that the disordered nucleosomes could be reorganized into 30 nm fibers under low-salt, diluted conditions. It is not only an important prediction by the polymer melt model but also a possible explanation for the observation of 30 nm chromatin fiber in so many earlier studies.

Combined with previous *in vivo* studies on *O. tauri* chromatin organization, we concluded that the interactions between nucleosomes in *O. tauri* resemble the interactions described by the polymer melt model. *In vivo*, the nucleosomes are highly condensed. (It should be noticed that “condensed” here only means that the average distances between nucleosomes are quite small. It is different from “compacted”, which implies an ordered organizing form. A “compacted” conformation can be less “condensed” than a disordered conformation.) The high concentration is maintained by the small nuclear volume and stabilized by the electrostatic interaction between nucleosomes and cations bound to chromatin. Because of the high condensation state of nucleosomes, the inter- and intra- 10 nm fiber interactions cannot be



distinguished *in vivo*. Thus, the nucleosomes inside the confined volume of a nucleus are in a disorganized state and no large-scale higher order structure is formed either in interphase cells or in mitotic cells.

We can use  $A_c$  and  $R_c$  (the subscript *c* means *cis*) to represent attractive force and repulsive force between interacting nucleosomes in the same 10 nm fiber and  $A_t$  and  $R_t$  (the subscript *t* means *trans*) to represent attractive force and repulsive force between interacting nucleosomes from different 10 nm fibers. *In vivo*, the nucleosomes are so close to each other that no matter whether interacting nucleosomes come from the same 10nm chromatin fiber or from different fibers, the interaction forces between the nucleosomes are indistinguishable. That means *in vivo*  $A_c + R_c = A_t + R_t$  (Figure 25).

Under artificial conditions, where the chromatin is released from the confinement of the small nuclear volume and the salt concentration is low compared to the salt concentration inside the nucleus, the chromatin can reorganize into the 30 nm fiber structure. If we use  $A_c'$ ,  $R_c'$ ,  $A_t'$  and  $R_t'$  to represent the forces between interacting nucleosomes after dilution in low-salt buffer, then  $A_c' + R_c' \gg A_t' + R_t'$ . The *in vitro* low-salt condition will immediately lead to  $R_c' > R_c$ , because less negative charges of DNA are neutralized. The interacting nucleosomes inside the same 10 nm fiber will repel each other and

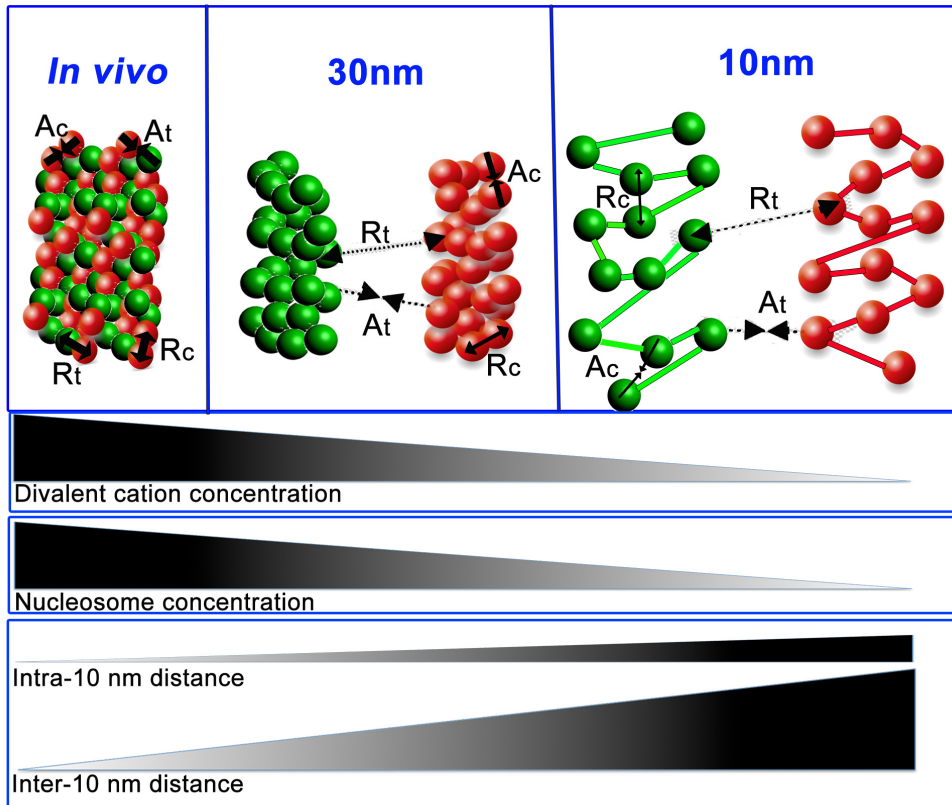


**Figure 25. Chromatin conformation at different conditions.**

For *In vivo* polymer melt conformation, nucleosome concentration is quite high. Intra- and inter- 10 nm fiber forces cannot be distinguished. Nucleosomes are most condensed at this state. For 30 nm fiber conformation, nucleosomes are in a diluted state. Intra-10 nm fiber forces become dominant. Inter-10 nm forces have a minor effect on chromatin conformation, thus are shown by dashed arrows. For 10 nm fiber conformation, chromatin is almost completely stripped of divalent cations. Nucleosomes are most decondensed at this state. The thickness of arrows are only schematically drawn to represent the difference in magnitude between different forces.

reorganize until  $R_c' < A_c'$  (Figure 25). Now the previously disordered but highly condensed nucleosomes may fold into a compact but less condensed structure like 30 nm chromatin fiber. Because under the diluted, low-salt condition, this higher-order structure is the most stable conformation. It should be noted that previous *in vitro* studies where the

30 nm chromatin fiber could be detected were all carried out under such artificial conditions.

The results from cryo-EM studies suggest that 30 nm fibers do not exist on a large-scale *in vivo*. However, the polymer melt model also implies that the nucleosomes are highly dynamic. In the “sea” of nucleosomes, the interactions between nucleosomes may change locally and transiently. Our data show that *O. tauri* chromatin is able to form higher order structure and also support the idea that the change of chromatin organization can potentially be used by the cell as a regulation mechanism for transcription, DNA replication and other chromatin-related cell activities. The flexible nature of nucleosome fibers in cells implies that a population with any structure or conformation can exist at any time, according to Tremethick [37]. Due to the low contrast and low signal to noise ratio of cryo-EM images, it is very hard to resolve small-scale structural features (like sparsely distributed 30 nm chromatin fibers) in the crowded milieu of the nucleus. Thus, although cryo-EM fails to detect any large-scale higher order structure of chromatin in most eukaryotic cells, we cannot exclude the possibility that the 30 nm fiber structure, or any other chromatin higher order structure, may exist at a local level. In a summary, it is possible that varying organizations of nucleosomes at different time and different nuclear locations form a dynamic pool of chromatin structures that regulates chromatin functions.

## Chapter 4. Future Work

Compared to other eukaryotic cells like mammalian cells, the genome of *O. tauri* has many unique features. Due to the lack of some important information for *O. tauri*, such as the linker histone H1 sequence and the state of histone post-translational modifications, we cannot make the conclusion that chromatin organization in *O. tauri* can apply to other eukaryotic cells as well. To better evaluate results from *O. tauri* chromatin study, more work on *O. tauri* genome and histone composition is needed. Also, to solve the debate of the 30 nm chromatin fiber, more *in vivo* studies from different eukaryotic cells are needed. To confirm that the densities we focused on were indeed from *O. tauri* chromatin, besides our negative control using *O. tauri* treated with 5mM EDTA, a positive control is needed as well. Histone antibodies could be used to design an immuno-cryo-EM experiment as the positive control.

According to our present data, the resolution was not only high enough to identify chromatin higher order structures if the structure was formed, but also high enough to identify nucleosome densities and even linker DNA densities. Future quantitative characterization of the polymer melt model will be possible. The polymer melt model has the potential to predict chromatin conformational changes. Once the mechanism behind chromatin conformational change is known, the role

of chromatin structure in the regulation of transcription and DNA replication would be much better understood.

## References

- [1] Flemming W. Zellsubstanz, kern und zelltheilung: Vogel; 1882.
- [2] Luger K, Mader AW, Richmond RK, Sargent DF, Richmond TJ. Crystal structure of the nucleosome core particle at 2.8 angstrom resolution. *Nature* 1997;389:251-60.
- [3] Kornberg RD. Chromatin structure: a repeating unit of histones and DNA. *Science* 1974;184:868-71.
- [4] Shaw BR, Herman TM, Kovacic RT, Beaudreau GS, Van Holde K. Analysis of subunit organization in chicken erythrocyte chromatin. *Proceedings of the National Academy of Sciences* 1976;73:505-9.
- [5] Varshavsky AJ, Bakayev VV, Georgiev GP. Heterogeneity of chromatin subunits in vitro and location of histone H1. *Nucleic Acids Research* 1976;3:477-92.
- [6] Olins AL, Olins DE. Spheroid chromatin units (v bodies). *Science* 1974;183:330-2.
- [7] Finch JT, Klug A. Solenoidal model for superstructure in chromatin. *Proceedings of the National Academy of Sciences* 1976;73:1897-901.
- [8] Thoma F, Koller T, Klug A. Involvement of histone H1 in the organization of the nucleosome and of the salt-dependent superstructures of chromatin. *The Journal of Cell Biology* 1979;83:403-27.
- [9] Rattner JB, Hamkalo BA. Higher order structure in metaphase chromosomes. II. The relationship between the 250 A fiber, superbeads and beads-on-a-string. *Chromosoma* 1978;69:373-9.
- [10] McGhee JD, Rau DC, Charney E, Felsenfeld G. Orientation of the nucleosome within the higher order structure of chromatin. *Cell* 1980;22:87-96.
- [11] Bednar J, Horowitz RA, Dubochet J, Woodcock CL. Chromatin conformation and salt-induced compaction: three-dimensional structural information from cryoelectron microscopy. *The Journal of Cell Biology* 1995;131:1365-76.
- [12] Worcel A, Strogatz S, Riley D. Structure of chromatin and the linking number of DNA. *Proceedings of the National Academy of Sciences* 1981;78:1461-5.
- [13] Williams SP, Athey BD, Muglia LJ, Schappe RS, Gough AH, Langmore JP. Chromatin fibers are left-handed double helices with diameter and mass per unit length that depend on linker length. *Biophysical Journal* 1986;49:233-48.
- [14] Woodcock CL. Chromatin fibers observed in situ in frozen hydrated sections. Native fiber diameter is not correlated with nucleosome repeat length. *The Journal of Cell Biology* 1994;125:11-9.
- [15] Horowitz RA, Agard DA, Sedat JW, Woodcock CL. The three-dimensional architecture of chromatin in situ: electron tomography reveals fibers composed of a continuously variable zig-zag nucleosomal ribbon. *The Journal of Cell Biology* 1994;125:1-10.
- [16] Scheffer MP, Eltsov M, Frangakis AS. Evidence for short-range helical order in the 30-nm chromatin fibers of erythrocyte nuclei. *Proceedings of the National Academy of Sciences* 2011;108:16992-7.
- [17] Bednar J, Horowitz RA, Grigoryev SA, Carruthers LM, Hansen JC, Koster AJ, et al. Nucleosomes, linker DNA, and linker histone form a unique structural motif that directs the

- higher-order folding and compaction of chromatin. *Proceedings of the National Academy of Sciences* 1998;95:14173-8.
- [18] Fierz B, Chatterjee C, McGinty RK, Bar-Dagan M, Raleigh DP, Muir TW. Histone H2B ubiquitylation disrupts local and higher-order chromatin compaction. *Nat Chem Biol* 2011;7:113-9.
- [19] Strahl BD, Allis CD. The language of covalent histone modifications. *Nature* 2000;403:41-5.
- [20] Shogren-Knaak M, Ishii H, Sun J-M, Pazin MJ, Davie JR, Peterson CL. Histone H4-K16 acetylation controls chromatin structure and protein interactions. *Science* 2006;311:844-7.
- [21] Maeshima K, Hihara S, Eltsov M. Chromatin structure: does the 30-nm fibre exist in vivo? *Curr Opin Cell Biol* 2010;22:291-7.
- [22] Bak AL, Zeuthen J, Crick FH. Higher-order structure of human mitotic chromosomes. *Proceedings of the National Academy of Sciences* 1977;74:1595-9.
- [23] Marsden MPF, Laemmli UK. Metaphase chromosome structure: evidence for a radial loop model. *Cell* 1979;17:849-58.
- [24] Adolph KW. Organization of chromosomes in mitotic HeLa cells. *Experimental Cell Research* 1980;125:95-103.
- [25] Paulson JR, Laemmli UK. The structure of histone-depleted metaphase chromosomes. *Cell* 1977;12:817-28.
- [26] Andersson K, Mähr R, Björkroth B, Daneholt B. Rapid reformation of the thick chromosome fiber upon completion of RNA synthesis at the Balbiani ring genes in *Chironomus tentans*. *Chromosoma* 1982;87:33-48.
- [27] Reeves R. Transcriptionally active chromatin. *Biochimica et Biophysica Acta (BBA) - Gene Structure and Expression* 1984;782:343-93.
- [28] Noll M, Thomas JO, Kornberg RD. Preparation of native chromatin and damage caused by shearing. *Science* 1975;187:1203-6.
- [29] Woodcock CL, Frado LL, Rattner JB. The higher-order structure of chromatin: evidence for a helical ribbon arrangement. *The Journal of Cell Biology* 1984;99:42-52.
- [30] Yu Z, Gonciarz MD, Sundquist WI, Hill CP, Jensen GJ. Cryo-EM structure of dodecameric Vps4p and its 2:1 complex with Vta1p. *Journal of Molecular Biology* 2008;377:364-77.
- [31] Song F, Chen P, Sun D, Wang M, Dong L, Liang D, et al. Cryo-EM study of the chromatin fiber reveals a double helix twisted by tetranucleosomal units. *Science* 2014;344:376-80.
- [32] Simpson RT, Thoma F, Brubaker JM. Chromatin reconstituted from tandemly repeated cloned DNA fragments and core histones: a model system for study of higher order structure. *Cell* 1985;42:799-808.
- [33] Lowary PT, Widom J. New DNA sequence rules for high affinity binding to histone octamer and sequence-directed nucleosome positioning. *Journal of Molecular Biology* 1998;276:19-42.
- [34] Huynh VAT, Robinson PJJ, Rhodes D. A method for the in vitro reconstitution of a defined "30nm" chromatin fibre containing stoichiometric amounts of the linker histone. *Journal of Molecular Biology* 2005;345:957-68.
- [35] Grigoryev SA, Arya G, Correll S, Woodcock CL, Schlick T. Evidence for heteromorphic chromatin fibers from analysis of nucleosome interactions. *Proceedings of the National Academy of Sciences* 2009;106:13317-22.

- [36] Robinson PJJ, Fairall L, Huynh VAT, Rhodes D. EM measurements define the dimensions of the “30-nm” chromatin fiber: evidence for a compact, interdigitated structure. *Proceedings of the National Academy of Sciences* 2006;103:6506-11.
- [37] Tremethick DJ. Higher-order structures of chromatin: the elusive 30 nm fiber. *Cell* 2007;128:651-4.
- [38] Schalch T, Duda S, Sargent DF, Richmond TJ. X-ray structure of a tetranucleosome and its implications for the chromatin fibre. *Nature* 2005;436:138-41.
- [39] Hardin J, Bertoni G, Kleinsmith LJ. *Becker's World of the Cell*: Benjamin Cummings; 2012.
- [40] Karp G. *Cell Biology: International Student Version*: John Wiley and Sons; 2010.
- [41] Lodish H. *Molecular cell biology*: Macmillan; 2008.
- [42] Butler PJ. A defined structure of the 30 nm chromatin fibre which accommodates different nucleosomal repeat lengths. *EMBO J* 1984;3:2599-604.
- [43] Clapier CR, Cairns BR. The biology of chromatin remodeling complexes. *Annu Rev Biochem* 2009;78:273-304.
- [44] Giannasca PJ, Horowitz RA, Woodcock CL. Transitions between in situ and isolated chromatin. *Journal of Cell Science* 1993;105 ( Pt 2):551-61.
- [45] Varga-Weisz PD, Becker PB. Regulation of higher-order chromatin structures by nucleosome-remodelling factors. *Current Opinion in Genetics & Development* 2006;16:151-6.
- [46] Saha A, Wittmeyer J, Cairns BR. Chromatin remodelling: the industrial revolution of DNA around histones. *Nature Reviews Molecular Cell Biology* 2006;7:437-47.
- [47] Tsukiyama T, Daniel C, Tamkun J, Wu C. ISWI, a member of the SWI2/SNF2 ATPase family, encodes the 140 kDa subunit of the nucleosome remodeling factor. *Cell* 1995;83:1021-6.
- [48] Luijsterburg MS, White MF, van Driel R, Dame RT. The major architects of chromatin: architectural proteins in bacteria, archaea and eukaryotes. *Critical Reviews in Biochemistry and Molecular Biology* 2008;43:393-418.
- [49] Bustin M, Reeves R. High-mobility-group chromosomal proteins: architectural components that facilitate chromatin function. *Progress in nucleic acid research and molecular biology* 1996;54:35-100b.
- [50] Dubochet J. Twisting in a crowd. *Trends Cell Biol* 1993;3:1-3.
- [51] Strick R, Strissel PL, Gavrilov K, Levi-Setti R. Cation–chromatin binding as shown by ion microscopy is essential for the structural integrity of chromosomes. *The Journal of Cell Biology* 2001;155:899-910.
- [52] Maeshima K, Imai R, Tamura S, Nozaki T. Chromatin as dynamic 10-nm fibers. *Chromosoma* 2014;123:225-37.
- [53] Morgan JE, Blankenship JW, Matthews HR. Polyamines and acetylpolyamines increase the stability and alter the conformation of nucleosome core particles. *Biochemistry* 1987;26:3643-9.
- [54] Wells DE. Compilation analysis of histones and histone genes. *Nucleic Acids Research* 1986;14:r119-r49.
- [55] Williams AF. DNA synthesis in purified populations of avian erythroid cells. *Journal of Cell Science* 1972;10:27-46.



- [56] Cameron IL, Prescott DM. RNA and protein metabolism in the maturation of the nucleated chicken erythrocyte. *Experimental Cell Research* 1963;30:609-12.
- [57] Grigoryev SA, Woodcock CL. Chromatin organization — The 30nm fiber. *Experimental Cell Research* 2012;318:1448-55.
- [58] Christen R, Schackmann RW, Shapiro BM. Metabolism of sea urchin sperm. Interrelationships between intracellular pH, ATPase activity, and mitochondrial respiration. *Journal of Biological Chemistry* 1983;258:5392-9.
- [59] Weintraub H. The nucleosome repeat length increases during erythropoiesis in the chick. *Nucleic Acids Research* 1978;5:1179-88.
- [60] Kowalski A, Pałyga J. Chromatin compaction in terminally differentiated avian blood cells: the role of linker histone H5 and non-histone protein MENT. *Chromosome Res* 2011;19:579-90.
- [61] Brotherton TW, Covault J, Shires A, Chalkley R. Only a small fraction of avian erythrocyte histone is involved in ongoing acetylation. *Nucleic Acids Research* 1981;9:5061-73.
- [62] Tobin RS, Seligy VL. Characterization of chromatin-bound erythrocyte histone V (f2c). Synthesis, acetylation, and phosphorylation. *the journal of biological chemistry* 1975;250:358-64.
- [63] Palau J, Ruiz-Carrillo A, Subirana JA. Histones from sperm of the sea urchin *Arbacia lixula*. *Eur J Biochem* 1969;7:209-13.
- [64] Crane-Robinson C, Dancy SE, Bradbury EM, Garel A, Kovacs AM, Champagne M, et al. Structural studies of chicken erythrocyte histone H5. *Eur J Biochem* 1976;67:379-88.
- [65] Compton JL, Bellard M, Chambon P. Biochemical evidence of variability in the DNA repeat length in the chromatin of higher eukaryotes. *Proceedings of the National Academy of Sciences* 1976;73:4382-6.
- [66] Spadafora C, Bellard M, Lee Compton J, Chambon P. The DNA repeat lengths in chromatins from sea urchin sperm and gastrula cells are markedly different. *FEBS letters* 1976;69:281-5.
- [67] Grummt I. Regulation of mammalian ribosomal gene transcription by RNA polymerase I. *Progress in nucleic acid research and molecular biology* 1998;62:109-54.
- [68] Hamperl S, Wittner M, Babl V, Perez-Fernandez J, Tschochner H, Griesenbeck J. Chromatin states at ribosomal DNA loci. *BBA - Gene Regulatory Mechanisms* 2013;1829:405-17.
- [69] Kaplan N, Hughes TR, Lieb JD, Widom J, Segal E. Contribution of histone sequence preferences to nucleosome organization: proposed definitions and methodology. *Genome Biol* 2010;11:140.
- [70] Gencheva M, Boa S, Fraser R, Simmen MW, A. Whitelaw CB, Allan J. In vitro and in vivo nucleosome positioning on the ovine  $\beta$ -Lactoglobulin gene are related. *Journal of Molecular Biology* 2006;361:216-30.
- [71] Thåström A, Bingham LM, Widom J. Nucleosomal locations of dominant DNA sequence motifs for histone–DNA interactions and nucleosome positioning. *Journal of Molecular Biology* 2004;338:695-709.
- [72] Kaplan N, Moore IK, Fondufe-Mittendorf Y, Gossett AJ, Tillo D, Field Y, et al. The DNA-encoded nucleosome organization of a eukaryotic genome. *Nature* 2008;458:362-6.

- [73] Sung MT, Wagner TE, Hartford JB, Serra M, Vandegriff V. Phosphorylation and dephosphorylation of histone V (H5): controlled condensation of avian erythrocyte chromatin. Appendix: Phosphorylation and dephosphorylation of histone H5. II. Circular dichroic studies. *Biochemistry* 1977;16:286-90.
- [74] Peterson CL, Laniel M-A. Histones and histone modifications. *Current Biology* 2004;14:R546-R51.
- [75] Rothbart SB, Strahl BD. Interpreting the language of histone and DNA modifications. *BBA - Gene Regulatory Mechanisms* 2014;1839:627-43.
- [76] Griffiths G. Electron Microscopy in Cell Biology. *Encyclopedia of Molecular Cell Biology and Molecular Medicine: Wiley-VCH Verlag GmbH & Co. KGaA*; 2006.
- [77] Ayache J, Beaunier L, Boumendil J, Ehret G, Laub D. Artifacts in Transmission Electron Microscopy. *Sample Preparation Handbook for Transmission Electron Microscopy: Springer New York*; 2010. p. 125-70.
- [78] Rasmussen N. Facts, artifacts, and mesosomes: Practicing epistemology with the electron microscope. *Studies in History and Philosophy of Science Part A*;24:227-65.
- [79] Hopwood D. Theoretical and practical aspects of glutaraldehyde fixation. *Histochem J* 1972;4:267-303.
- [80] Jansen EF, Tomimatsu Y, Olson AC. Cross-linking of  $\alpha$ -chymotrypsin and other proteins by reaction with glutaraldehyde. *Archives of Biochemistry and Biophysics* 1971;144:394-400.
- [81] Quijoch FA, Richards FM. The enzymic behavior of carboxypeptidase-A in the solid state\*. *Biochemistry* 1966;5:4062-76.
- [82] Mirzabekov AD, Shick VV, Belyavsky AV, Bavykin SG. Primary organization of nucleosome core particle of chromatin: sequence of histone arrangement along DNA. *Proceedings of the National Academy of Sciences* 1978;75:4184-8.
- [83] Mollenhauer HH. Artifacts caused by dehydration and epoxy embedding in transmission electron microscopy. *Microsc Res Tech* 1993;26:496-512.
- [84] Booy FP, Ruigrok RW, van Bruggen EF. Electron microscopy of influenza virus. A comparison of negatively stained and ice-embedded particles. *Journal of Molecular Biology* 1985;184:667-76.
- [85] Olins AL, Olins DE. Stereo electron microscopy of the 25-nm chromatin fibers in isolated nuclei. *The Journal of Cell Biology* 1979;81:260-5.
- [86] Dubochet J, Sartori Blanc N. The cell in absence of aggregation artifacts. *Micron* 2001;32:91-9.
- [87] Moor H. Theory and practice of high pressure freezing. *Cryotechniques in biological electron microscopy* 1987:175-91.
- [88] Gan L, Jensen GJ. Electron tomography of cells. *Quart Rev Biophys* 2012;45:27-56.
- [89] Frank J. Single-particle imaging of macromolecules by cryo-electron microscopy. *Annu Rev Biophys Biomol Struct* 2002;31:303-19.
- [90] Schroder RR, Manstein DJ, Jahn W, Holden H, Rayment I, Holmes KC, et al. Three-dimensional atomic model of F-actin decorated with Dictyostelium myosin S1. *Nature* 1993;364:171-4.

- [91] Rayment I, Holden HM, Whittaker M, Yohn CB, Lorenz M, Holmes KC, et al. Structure of the actin-myosin complex and its implications for muscle contraction. *Science* 1993;261:58-65.
- [92] Li X, Mooney P, Zheng S, Booth CR, Braunfeld MB, Gubbens S, et al. Electron counting and beam-induced motion correction enable near-atomic-resolution single-particle cryo-EM. *Nat Meth* 2013;10:584-90.
- [93] McDowell AW, Smith JM, Dubochet J. Cryo-electron microscopy of vitrified chromosomes in situ. *EMBO J* 1986;5:1395-402.
- [94] Bouchet-Marquis C, Dubochet J, Fakan S. Cryoelectron microscopy of vitrified sections: a new challenge for the analysis of functional nuclear architecture. *Histochem Cell Biol* 2005;125:43-51.
- [95] Eltsov M, MacLellan KM, Maeshima K, Frangakis AS, Dubochet J. Analysis of cryo-electron microscopy images does not support the existence of 30-nm chromatin fibers in mitotic chromosomes in situ. *Proceedings of the National Academy of Sciences* 2008;105:19732-7.
- [96] Weidemann T, Wachsmuth M, Knoch TA, Müller G, Waldeck W, Langowski J. Counting nucleosomes in living cells with a combination of fluorescence correlation spectroscopy and confocal imaging. *Journal of Molecular Biology* 2003;334:229-40.
- [97] Courties C, Vaquer A, Troussellier M, Lautier J, Chrétiennot-Dinet MJ, Neveux J, et al. Smallest eukaryotic organism. *Nature* 1994.
- [98] Derelle E, Ferraz C, Rombauts S, Rouzé P, Worden AZ, Robbens S, et al. Genome analysis of the smallest free-living eukaryote *Ostreococcus tauri* unveils many unique features. *Proceedings of the National Academy of Sciences* 2006;103:11647-52.
- [99] Farinas B, Mary C, de O Manes C-L, Bhaud Y, Peaucellier G, Moreau H. Natural synchronisation for the study of cell division in the green unicellular alga *Ostreococcus tauri*. *Plant Mol Biol* 2006;60:277-92.
- [100] Henderson GP, Gan L, Jensen GJ. 3-D ultrastructure of *O. tauri*: Electron cryotomography of an entire eukaryotic cell. *PLoS ONE* 2007;2:e749.
- [101] Gan L, Ladinsky MS, Jensen GJ. Chromatin in a marine picoeukaryote is a disordered assemblage of nucleosomes. *Chromosoma* 2013;122:377-86.
- [102] Tivol WF, Briegel A, Jensen GJ. An improved cryogen for plunge freezing. *Microsc Microanal* 2008;14:375-9.
- [103] Suloway C, Pulokas J, Fellmann D, Cheng A, Guerra F, Quispe J, et al. Automated molecular microscopy: the new Legimon system. *Journal of structural biology* 2005;151:41-60.
- [104] Mastronarde DN. Dual-axis tomography: an approach with alignment methods that preserve resolution. *Journal of structural biology* 1997;120:343-52.
- [105] Suau P, Bradbury EM, Baldwin JP. Higher - order structures of chromatin in solution. *European Journal of Biochemistry* 1979;97:593-602.
- [106] Bloomfield VA. DNA condensation by multivalent cations. *Biopolymers* 1997;44:269-82.